Virginia Commonwealth University
VCU Scholars Compass

Theses and Dissertations | Graduate School

2018

IMPROVING REALTIME 3-D TRACKING OF HIGH DOSE RATE RADIATION SOURCE USING A FLAT PANEL DETECTOR

Leo Uchechukwu Udeji

Follow this and additional works at: https://scholarscompass.vcu.edu/etd

 Part of the Biomedical Engineering and Bioengineering Commons

© The Author

Downloaded from
https://scholarscompass.vcu.edu/etd/5486

This Thesis is brought to you for free and open access by the Graduate School at VCU Scholars Compass. It has been accepted for inclusion in Theses and Dissertations by an authorized administrator of VCU Scholars Compass. For more information, please contact libcompass@vcu.edu.

VIRGINIA COMMONWEALTH UNIVERSITY

Virginia Commonwealth University
VCU Scholars Compass

Thesis and Dissertations **Graduate School**

2018

IMPROVING REALTIME 3-D TRACKING OF HIGH DOSE RATE RADIATION SOURCE USING A FLAT PANEL DETECTOR

Leo Uchechukwu Udeji

Virginia Commonwealth University

© Leo Uchechukwu Udeji 2018

All Rights Reserved

IMPROVING REALTIME 3-D TRACKING OF HIGH DOSE RATE RADIATION SOURCE USING A FLAT PANEL DETECTOR

A thesis submitted in partial fulfillment of the requirements for the degree of Master of Science at Virginia Commonwealth University.

By

LEO UCHECHUKWU UDEJI

Bachelor of Electronics Engineering, Infrastructure University Kuala Lumpur Malaysia 2014

Advisor: DING-YU FEI, PH.D.

ASSOCIATE PROFESSOR BIOMEDICAL ENGINEERING

Director: DORIN TODOR, PH.D.

ASSOCIATE PROFESSOR, RADIATION ONCOLOGY

Virginia Commonwealth University

Richmond, Virginia

May 2018

Acknowledgement

My sincerest appreciation to my advisor Dr Dorin A. Todor, for rendering all forms of assistance to me during the period of this research, and for guiding me through the intriguing process of understanding cancer treatment. It has been a magnificent experience working at VCU's Massey cancer center. I hope that our findings make considerable contributions towards the search for an effective and improved brachytherapy treatment process.

I would also like to specially thank my mentor and advisor, Dr Ding-Yu Fei, for choosing me to work on this research; for guiding and advising me on the best ways to meet my research goals and quickly record notable milestones within the shortest time possible, and for frequently checking-in on my progress. I appreciate your assistance during that period when I was overwhelmed with circumstances beyond my capacity. It has been a great experience working with you.

Not forgetting to thank committee members Dr Ruixin Niu and Dr Alen Docef, who took out time to explain to me what's expected of me and who occasionally advised me on ways to get out of problems I encountered in the course of this research.

Finally, I would like to thank God for giving me a wonderful and supportive family both in Nigeria and here in America (Mr and Mrs Jeffrey), that have gone through the thick and thin, to ensure that I complete my education; I can never thank them enough. Also to Dr Tripletts, who saved my education, at the point I thought it was all over; I say thank you.

Table of Contents

Page

List of Tables

Page

List of Figures

Page

List of Abbreviations

CT – Computed Tomography

LINAC - Linear accelerator

GUI – Graphical User Interface

FPD – Flat Panel Detector

HDR – High Dose Rate

QA – Quality Assurance

WBI- Whole Breast Irradiation

BCS-Breast Conservation Surgery

BCT-Breast Conservation Therapy

ACS – American Cancer Society

IBR - Ipsilateral Breast Relapse

APBI - Accelerated Partial Breast Irradiation

CTCA - Cancer Treatment Center of America

EBRT - External Beam Radiation Therapy

MIRT - Multicatheter Interstitial Brachytherapy

PTV - Planning Target Volume

OARs - Organs At Risk

IORT - Intraoperative Radiation Therapy

BED - Biological Effective Dose

MSB - MammoSite brachytherapy

IP – Internet Protocol

MEX – MATLAB Exchange File

DICOM - Digital Imaging and Communications in Medicine

MAC – Media Access Control

Abstract

Improving Realtime 3-D Tracking of High Dose Rate Radiation Source Using A Flat Panel Detector

By Leo Uchechukwu Udeji, B.E.E

A Thesis submitted in partial fulfillment of the requirements for the degree of Master of Science at Virginia Commonwealth University.

Virginia Commonwealth University, 2018

Advisor: Ding-Yu Fei, Ph.D.

Associate Professor, Biomedical Engineering

Major Director: Dorin Todor, Ph.D.

Associate Professor, Radiation Oncology

Previous research [1] on this subject tracked the presumed exact path the HDR source would follow in real-time, during breast brachytherapy treatments in other to ensure accurate dose delivery and effectively confirm actual source position. As a continuation, this research has three objectives. Firstly, we will extract information from patient DICOM file which will be used to perform evaluations, then we will establish communication between our C program and the new Varex Paxscan flat panel detector (FPD). Finally, we will try to embed our C codes into a

MATLAB graphical user interface (GUI) This research will attempt to improve the overall existing system in several ways including, code optimization and trying a sample simulation of the process in MATLAB guide app, to check the quality of the new design. Finally, all the algorithms will be integrated into the user-friendly GUI, such that its operation can be implemented easily. The FPD is used to obtain images resulting from the exit radiation of the HDR source, emerging from an organized matrix of markers. The images are processed using in-built functions in MATLAB to obtain projection coordinates, and marker coordinates. Each marker along with its projection constitutes a line in 3D. Using the mathematical solution for near intersection of two 3D lines, N-markers will produce N*(N-1)/2 points of intersection and their mean will produce a more precise source position. The changes in this position as well as the time interval between these changes will be used to confirm the accuracy of our treatment system using the standalone monitoring system built in this research. In the previous study the accuracy of source position detection using the FPD was found to be in sub-millimeter. This study which uses a new FPD with improved features is used to confirm that, but our focus here is improvement of the previous work, as stated earlier.

CHAPTER 1 INTRODUCTION

1.1 Background

In 1896 a German physics professor, Wilhelm Conrad Roentgen, presented lecture entitled "Concerning a New Kind of Ray". He called it the X-ray, with 'x' being the algebraic symbol for an unknown quantity. Months after this discovery, systems were being designed to use x-rays for diagnosis; in 3 years radiation was used to treat cancer[1].

In 1898 however, the discovery of radium by the Curie's introduced a compact source of unvarying highly penetrating rays suitable for external or internal applications. Radium was so rare and expensive in those early days that practitioners used trivial and less effective quantities. Mass global exploitation of radium in several continents resulted in sufficient availability for practical application. By 1920 radium-therapy had replaced surgery as the preferred treatment for gynecologic malignancy. Several years of study and evolution of this new technique led to reactor and cyclotron-produced radionuclides, with higher specific activity and lower γ-ray/photon energy. This has expanded applicability and patient safety. Computed dosimetry has improved the therapeutic ratio, and remote after-loading has eliminated radiation exposure to personnel [2].

Skeletal remains of a 2700-year-old Russian King and a 2200-year-old Egyptian mummy have both been diagnosed with prostate cancers[3]. These findings are proof that cancer has probably existed as long as humans. Breast cancer which is the focus of this research can also be traced back to 1600 BC Edwin Smith Papyrus, back in ancient Egypt. Since breast cancer is outwardly visible in its most advanced stage it was easy for our ancestors to notice it enough to record it. Throughout the ages, it has been difficult to ascertain the causes of breast cancer. Research continues still, today.

Breast brachytherapy is a radiation therapy procedure used in modern times after lumpectomy, as part of breast conservation solution.

1.2 Objective of the Study

Several techniques used to monitor the performance of cancer treatment via external beam radiation already exists. Unfortunately, they don't exist for high dose rate (HDR) brachytherapy. High dose rate brachytherapy according to cancer treatment center of America is a type of internal radiation therapy that delivers radiation from implants placed close to, or inside the tumors in the body. This research seeks to address this problem using a MATLAB based standalone monitoring system.

This study is very important for two main reasons: firstly, nothing like this exists, and mistakes made during radiation therapy can be very costly especially for the patient. The final product from this research will help radiation therapists meet the quality assurance standards set by the nuclear regulatory commission (NRC).

CHAPTER 2 BACKGROUND

2.1 Breast Cancer

Cancer is the name given to a collection of malignant and related diseases, which can start almost anywhere in the human body[3]. In all types of cancer, some of the body's cells begin to divide without stopping and spread to surrounding tissues. Cancer is a genetic disease that is caused by changes to the genes that control the way our cells function, especially how they grow and divide. Breast cancer is a disease characterized by growth of malignant cells in the mammary glands. It can strike both males and females; but research shows that women are about 100times more likely to develop the disease than men[4]. Most incidents of cancer in female breasts form shortly before, during, or after menopause, with three-quarter of all cases being diagnosed after the age 50. Generally older women are more likely to develop breast cancer[4]. In the 20th and 21st centuries breast cancer was the leading cause of death among women worldwide but by 2012, this only remained true in less developed countries. In high income countries lung cancer has overtaken breast cancer as the leading cause of death among women. Breast cancer accounts for 10.4% of all cancer incidence among women, making it the second most common type of non-skin cancer (after lung cancer) and the fifth most common cause of cancer death[10]. In the USA breast cancer has the highest incidence among all cancer types in females with one in every eight to ten women being affected during her lifetime; it was estimated that 192,370 women will be diagnosed with, and 40,170 women will die of, cancer of the breast in 2009. In the UK breast cancer is the most common among women, although it is rare in men[10]. For example, in the UK, in 2006 there were 45,822 new cases of breast cancer diagnosed; 45,508(over 99%) in women and 314(less than 1%) in men. It has been estimated that the lifetime risk of developing breast cancer is 1 in 1014 for men and 1 in 9 for women in the UK[10].

Given that there are several types of breast cancer, the exact causes of breast cancer is unknown till date; but it is known that both environmental and genetic factors are involved, such as specified mutations in HER2, BRCA1, BRCA2, CHEK2 and p53 genes, which may be inherited[4] or a product of evolution[5].

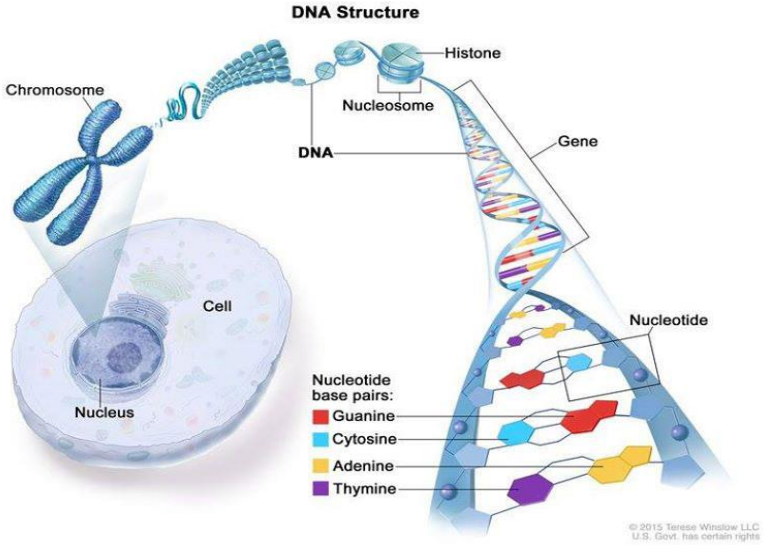

Figure 1: Image showing the basic physical units of inheritance. Genes are arranged in long strands of tightly packed DNA called Chromosomes[24].

2.2 Treatment and Prevention of Breast Cancer

Breast cancer dates to the prehistoric era; with its first case been assumed to have been seen in Egypt. It was found in the remains of mummies and was also documented in ancient manuscripts[1]. The earliest record of breast cancer was found in Edwin Smith Surgical Papyrus, believed to have been written in the Egyptian pyramid Age. In these documents cancer was described as incurable. Burning the tumor or excising it using a knife was the treatment then. This didn't cure cancer since cancer is malignant. The tumor would normally reoccur in the same (ipsilateral) or different spot in the body.

The renaissance era witnessed advances in surgical procedures which led to a better understanding of the human body via autopsy. The anatomy of the breast was later described by Andreas Vesalius, which laid the foundation for the treatment of breast cancer[1]. Up until the 18th century surgeons amputated the breast as a form of treatment; but surgical conditions improved in 1846 when Morton discovered anesthesia[1]. In 1894 Halsted published his work, which was widely accepted by surgeons in the late 19th century to become the standard for the treatment of breast cancer for the next one hundred years. This method was called the Halsted radical mastectomy. In 1912 Murphy abandoned the Halsted operation, and developed a new method which did not include the removal of the pectoral muscle. This approach marked the beginning of the modified radical mastectomy; various clinical trials in the mid 1900's proved this method to be as effective as radical mastectomy for early stage breast cancer[1].

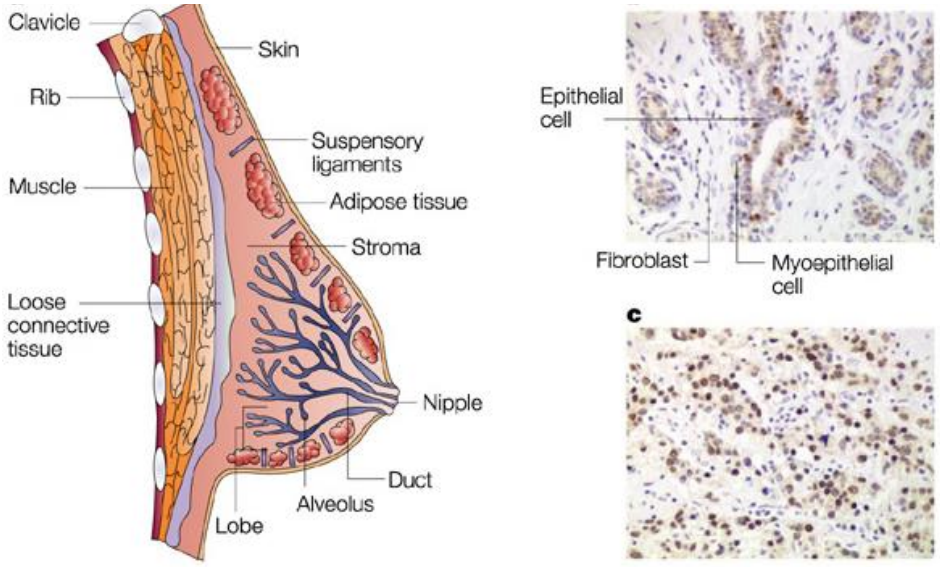

Figure 2: Structure of the human breast

Breast cancer has a remarkably high five-year survival rate. Early diagnosis via processes like self-examination or mammography, greatly improves the odds of survival. Survival rates is lower for cancer that have spread locally, and exceptionally low for cancers that have metastasized or spread to distant body parts[4].

Treatment of breast cancer after it is discovered to be malignant may entail surgery, radiation, or chemotherapy. Biological treatment is equally an option. Surgery is often the first method of treatment and might come in the form of lumpectomy, which removes only the cancerous mass and a small amount of surrounding tissue, or mastectomy which removes the entire breast. A modified radical mastectomy removes the breast along with adjacent lymph nodes. Side effects associated with surgery includes: changes in arm or shoulder mobility, swelling, infection, numbness, and when the lymph nodes are taken, fluid builds up in the region that they were taken from. Lumpectomy or mastectomy is usually followed by cosmetic or reconstructive surgery[4].

Currently, there's no known way to completely prevent breast cancer, but the risk of developing advanced disease can be reduced[4]. Prevention techniques includes: maintaining a healthy body weight, reducing alcohol consumption, and ceasing to smoke. Self-examination as well as professional annually mammogram is recommended for women aged 40 and older, while for women between 20 and 39years, mammogram is recommended every 3years. In some special cases, women who are at extreme risk due to strong family history or the presence of mutated BRCA genes, may opt for preventive mastectomy.

2.3 Radiation Therapy and Other Less Invasive Treatment Techniques

Radiation therapy, chemotherapy and biological therapy are less-invasive treatments for breast cancer[6]. Radiation therapy is usually employed to shrink tumors before surgery or to destroy small amounts of cancerous tissues remaining after surgery. The side effects after radiation includes: swelling, or thickening of the breast, vomiting, diarrhea, or skin irritations resembling sunburn [4]. Chemotherapy involves the use of chemicals to destroy cancerous cells, but this method is also known to attack normal cells, to some degree, causing side effects that include hair loss, immune suppression, mouth sores, fatigue, and nausea. Biological therapy entails the use of chemical inhibitors to block the hormones that stimulate growth of cancer cells.

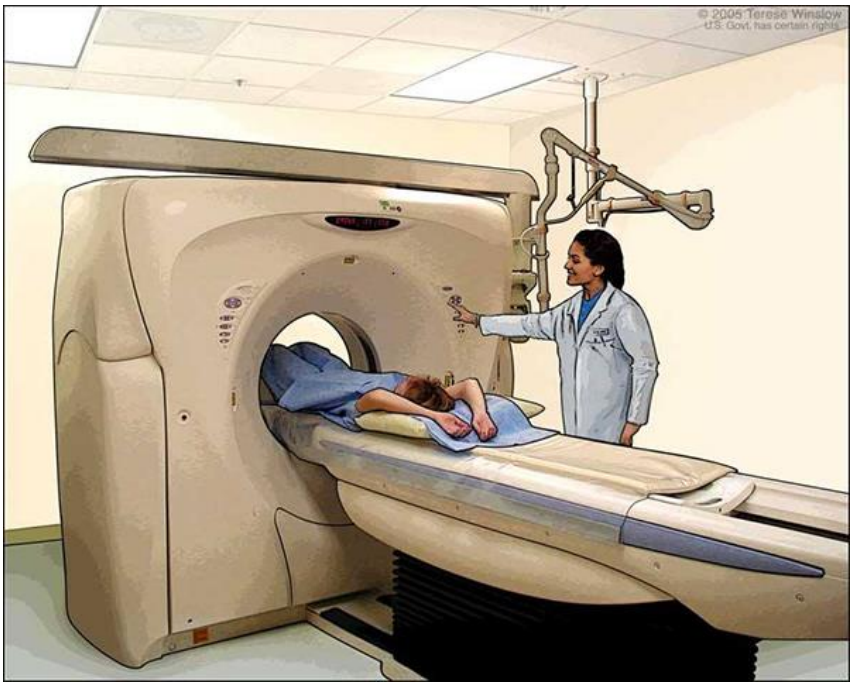

Figure 3: Computed Tomography Scanner(CT). CT scanners are often used in both radiation therapy and brachytherapy to obtain treatment plan information[24].

To implement radiation therapy, CT scanners are used to obtain pictures of the inside of the body via a computer connected to an x-ray machine[24]. Currently, there are several external beam radiation techniques in existence, each suited for a treatment depending on treatment goals.

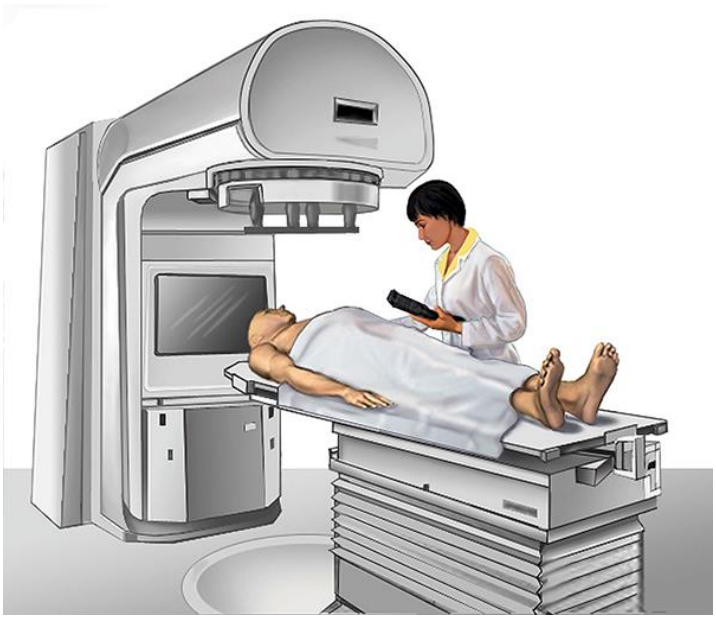

Figure 4: Linear accelerator (LINAC) used for external beam radiation therapy[24].

2.4 Breast Conservation Surgery (BCS) Followed By Radiation Therapy (RT)

According to American Cancer Society (ACS), breast conservation surgery/treatment (BCS) is an operation to remove the cancer while leaving as much normal breast as possible[2]. At times some surrounding healthy tissues and lymph nodes are usually also removed. The amount of breast removed depends on the several factors like the size and location of the tumor. Breast-conserving surgery is sometimes called lumpectomy, quadrantectomy, partial mastectomy, or segmental mastectomy. This technique is usually an option for in patient in the early stages of cancer. At the completion of lumpectomy, a pathologist will use a microscope to look at the edges of the removed tissues. If no cancer cells are found at any of the edges of the removed tissue, it is said to have negative or clear margins. The presence of positive margins means that some cancer cells may still be in the breast after surgery, so the surgeon might need to remove more tissue in an operation called re-excision. If at the end of this second surgery, cancer cells are still found then a mastectomy might be needed.

The advantages of BCS includes: it allows a woman keep most of her breast which will also require the application of more radiation via brachytherapy or radiation therapy, given by a radiation oncologist (doctor who specializes in radiation).

The side effects of this may include pain, a scar and/or dimple where the tumor was removed, a firm or hard surgical scar (Fibrosis), and sometimes lymphedema, a type of swelling in the arm[2].

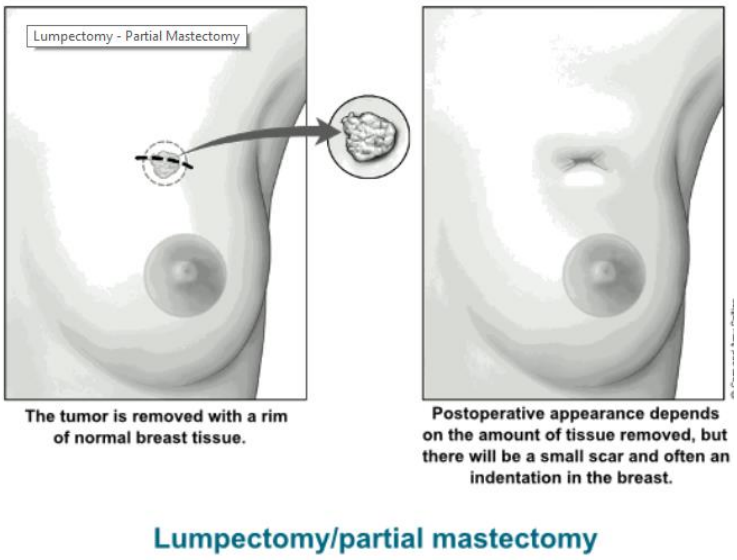

Figure 5: After effect of lumpectomy/partial mastectomy

Patients that desire breast reconstruction are usually advised to talk to their doctor before the surgery[2].

Several studies have been done on breast conservation surgery to study long term effect on patient body and the possibility of reoccurrence. In one study[7], a nomogram was used to predict the 10year ipsilateral breast relapse (IBR) after breast-conserving therapy (BCT) for breast cancer was developed based on the boost-no-boost trial with a concordance probability estimate (CPE) of 0.68. The aim of this project was to validate that algorithm. 1787 breast cancer cases, treated with BCT and radiotherapy from 2000 to 2007, at the University Hospitals Leuven were identified without missing data of the nomogram variables. Clinicopathological factors were assessed, as well as the validity of the prediction model in term of discrimination and calibration.

The median follow-up time used in this research was 10.75years. The 10year IBR rate was 1.4%. This research concluded that the predictive model for IBR in breast cancer didn't work, in this more recent study population. In another study[8], researchers perform a study to compare outcomes after breast conservation treatment with Iridium-192 implant boost versus electron boost (Brachy boost is the administration of lower dose[10-25Gy], implantable radiation in addition to external beam radiation of 45-70Gy [2]). Data of 141 patients treated via whole breast brachytherapy followed by iridium-192 boost after BCS between 1977 and 1983, were gotten and matched 1:1 to patients treated with electron boost. Outcome measures included survival, local reoccurrence, cosmesis, and complications. Median follow-up was 16.7 and 12.6years for

the implant versus electron group. The rate of reoccurrence, freedom from distant metastases and overall survival at 10/20years did not differ between the groups nor did patterns of first failure. Patients in the electron group were found more likely to have good/excellent cosmesis than those in the implant group 1year after radiotherapy. This trend continued through 10years but didn't reach statistical significance at years 5/10. Complications rates were similar although patients receiving electron boost seemed less likely to develop breast fibrosis than did those receiving implant boost (23/141 vs 58/141, respectively, incidence rate ratio 0.7). The conclusion from this research from a 20year data was that, there was no difference in the rate of local occurrence, freedom from distant metastases, overall survival, or patterns of failure between groups treated with these two well-described radiotherapy boost techniques. Better cosmesis was observed in the electron group in 1year after radiotherapy, with a trend continuing for 10years. The incidence of complication was similar between the groups, with a trend toward increased fibrosis in patients receiving implant boost. In a third study[9], which was done to report the 2year cosmetic outcome of a randomized trial comparing prone and supine whole-breast irradiation in large-breasted patients, one hundred patients with cup size>=C (European) were included. Before and 2-years after radiation therapy, clinical endpoints were scored, and digital photographs were taken with the arms alongside the body and with the arms elevated 180degrees. Three observers rate the photographs using the 4-point Harvard cosmesis scale. Cosmesis was also evaluated with the commercially available breast cancer conservation treatment / cosmetics results software (BCCT.core). Two-year follow-up data and photographs were available for 94 patients (47 supine treated and 47 prone treated). Patient and treatment characteristics were not significantly different between the 2 cohorts, with a worsening of color change occurring more frequently in the supine than in the prone cohort (19/46 vs 10/46 patients respectively). Five patients in the prone group which made up 11% of the group's population and 12 patients from the supine group which made-up 26% of the group's population, presented with a worse scoring of edema at 2-year follow-up. For retraction and fibrosis, no significant differences were found between the 2 cohorts, although scores were generally worse in the supine cohort. The cosmetic scoring by 3 observers did not reveal differences between the prone and supine groups. On the photographs with their hands up, seven patients in the supine group versus none in the prone group had a worsening of cosmesis of 2 categories using the BCCT.org software.

All in all, breast conservation surgery followed by brachytherapy are particularly important aspects of breast cancer treatment, after which patient caregivers are given instructions on how to care for the surgery site after surgery[2]. Caregiver instructions includes but are not limited to: how to care for the surgery site and dressing, how to care for your drain if you have one(a plastic rubber tube coming out of the surgery site that removes the fluid that collects during healing), how to recognize signs of infection, bathing and showering after surgery, when to call the doctor or nurse, when to start using your arm again and how to exercise the arm to avoid stiffness, when

you can start wearing a bra again, what to eat and not to eat, use of medicines including pain medicine and antibiotics, any restrictions on activity, what to expect regarding sensations of numbness in the breast and arm, what to expect regarding feelings about body image, when to see your doctor for a follow-up appointment, and referral to reach to recovery volunteer.

2.5 Accelerated Partial Breast Irradiation

Accelerated partial breast irradiation (APBI) according to cancer treatment center of America (CTCA) is a breast radiation therapy in which focused radiation is delivered specifically to the part of the breast where tumor is removed[11]. APBI treatment can be administered via brachytherapy or through external beam techniques, such as tomotherapy. APBI is normally an option when treatment involves: a small tumor, there is a clear surgical margin after a lumpectomy and preferably no lymph nodes containing cancer. It's a preferable option for women with early stage breast cancer[11].

Various approaches for APBI have been developed, they include[10]: multicatheter interstitial brachytherapy, balloon catheter brachytherapy, conformal external beam radiation therapy, and intraoperative radiation therapy (IORT).

Some advantages of APBI for breast cancer includes[11]:

- With APBI, breast radiation therapy treatments are focused specifically on the part of the breast where the tumor was removed, so radiation is contained to the tumor cavity as much as possible.
- Because radiation is so targeted, it affects less of the healthy tissue and organs close to the breasts, including the lungs, heart, ribs, muscles and skin.
- APBI can be given in a more condensed schedule than some other radiation therapies for breast cancer (5days instead of 6 to 7weeks).

One technique that like APBI is intensity modulated radiation therapy (IMRT); the only difference being that it applies beam from an external source (External Beam Radiation Therapy-EBRT), rather than via brachytherapy which is the subject of this research. This technique is sometimes recommended by the care-team based on patient plan and individual needs. It's usually administered for people who've had previous breast cancer radiation therapy and are experiencing recurrent tumors in the treatment area[11]. Some of its advantages includes [11]:

- IMRT employs an advanced computer program to accurately map your radiation dosage in 3-dimensionss, based on the breast tumor size, shape and location. It uses advanced technology to manipulate photon and photon beams of radiation to conform to the shape of the tumor.

- IMRT directs radiation at the breast tumor and modulates the intensity of the radiation beams, helping to spare healthy tissues surrounding the breast tumor.

- IMRT allows each dose of radiation to be custom-tailored according to the geographical shape of the breast tumor.

2.6 Brachytherapy and Breast Brachytherapy

The word brachy means short distance in Greek. Brachytherapy is a type of internal radiation therapy which uses a high activity source of short-range radiation such as Ir-192 sealed (enclosed within a capsule) and placed inside or close to the treatment location, to destroy cancer cells and shrink tumors[17]. This technique allows doctors to deliver higher doses of radiation to more specific areas of the body, compared with other conventional forms of radiation therapy such as external beam radiation where radiation is projected from a machine outside of the body. It is usually performed on outpatient basis. The advantages of brachytherapy include: fewer side effects as compared to some external beam radiation techniques since less healthy tissues are exposed, overall shorter treatment time (HDR) which helps reduce the chances of surviving cancer cells to divide and grow between each radiotherapy dose interval, and stability, in the sense that even when the patient moves during treatment the radiation sources retain their correct position in relation to the tumor. In 1929 Geofrey Kenynes was the first to publish results with brachytherapy used as the only method of treatment[1].

The methods used to deliver breast brachytherapy includes: interstitial breast brachytherapy, intracavitary breast brachytherapy (balloon brachytherapy), intraoperative radiation therapy, permanent breast seed implantation, and non-invasive brachytherapy which uses mammography for target localization and a HDR source. Dose rate in brachytherapy is usually measured in grays per unit time such as grays per hour (gy/hr) . A treatment is usually classified as high dose rate when it exceeds 12Gy/hr.

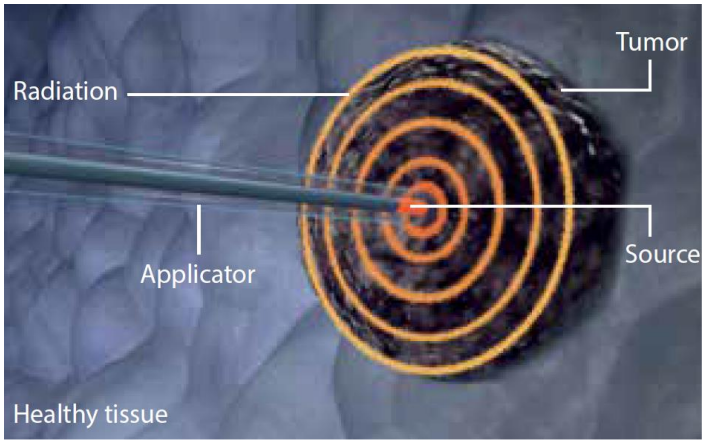

Figure 6: Concept of Brachytherapy[4].

Computed Tomography (CT) images are used to obtain information about treatment location. But it doesn't provide information about the unique size and shape of the tumor, or even the organ at risk (OAR)[16]. This could lead to tumor under-dosage or over-dosage which increases the chances of cancer cells reoccurring. The success or failure of HDR brachytherapy is therefore determined by the exact position of the radioactive source used in treatment. Accurate or optimal positioning of the source is essential for delivering the desired dose to the target area while avoiding injury to neighboring tissues. Optimal dose delivery depends among other things on the accuracy of catheter placement[17].

2.6.1 Multicatheter Interstitial Brachytherapy (MIB)

There are several brachytherapy techniques in existences, namely: interstitial implants, intracavitary devices with single/multilumen balloons, hybrid applicators, and irradiation with low energy x-ray. Of all APBI techniques currently, multicatheter interstitial brachytherapy (MIRT) has the longest follow-up and has a level 1 evidence as a valid treatment alternative to whole breast irradiation after breast conserving surgery (BCS)[12]. It involves the use of multiple catheters to administer radiation to a cancer tumor. This technique was initially developed to provide boost radiation after whole breast radiation therapy[10]. Flexible after-loading catheters are placed through the breast tissues surrounding the lumpectomy. The catheters are inserted at 1 to 1.5cm intervals in several planes; firstly to ensure adequate coverage of the lumpectomy cavity plus margins, and secondly to avoid hot and cold spots (areas of too much and too little irradiation respectively)[10]. Multiple catheters are placed in the breast using a free-hand or template-guided approach[10]. Catheter insertion requires a high level of experience to produce an implant of excellent quality. In MIB, either low-dose-rate(LDR) or high-dose-rate(HDR)

brachytherapy may be used. With LDR, sources of Ir-192 sources are implanted for approximately 2 to 5days while the patient is admitted as an inpatient. High Dose Rate (HDR) however, which we use in this research is an outpatient procedure, fractionated over the course of a week, with each treatment varying between seconds to minutes[10]. The dose used is usually based on biological effective dose (BED).

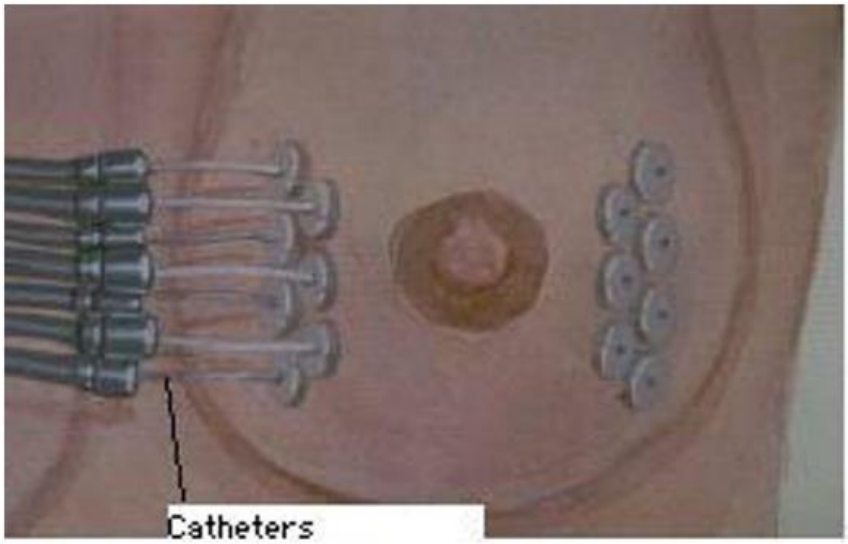

Figure 7: Illustration of multi-catheter interstitial brachytherapy[10].

To plan the right positions for the catheters, ultrasound or computed tomography (CT) imaging can be used, but the treatment plan is always based on postimplant CT images[12]. With CT imaging, the 3D target volume can be defined more precisely and delineation of the organs at risk volumes is also possible. Parameters calculated from dose-volume histogram can be used for quantitative plan evaluation. The catheter reconstruction is also easier and faster on CT images compared to X-ray films. In high dose rate brachytherapy, using a stepping source, several forward dose optimization methods (manual, geometrical, on dose points, graphical) are available to shape the dose distribution to the target volume, and these influence dose homogeneities to different extent. Currently, inverse optimization algorithms offer new possibilities to improve dose distribution further considering the requirements for dose coverage, dose homogeneity, and dose to organs at risk simultaneously or automatically.

It is of utmost importance to place the catheters in the right positions. To get an acceptable dose distribution, the planning target volume (PTV) must be geometrically covered by the catheters. To achieve this different imaging methods can be used. With ultrasound guidance the deepest

needles can be inserted manually if the resection cavity is visible, and the rest of the catheters are placed with a template, which can ensure an even spacing between the catheters. Another approach is when the superficial needles are inserted as first under ultrasound guidance followed by the deeper needles with template guidance, but the artefacts from the shallow needles may cause visibility problem. If the needles are manually inserted using ultrasound imaging, the PTV contour and all entry and exit points must be marked on the skin surface to plan the needles distribution. However, the best method is when a 3D imaging with full anatomical information about the resection cavity, PTV, and organs at risk (OARs) is available before insertions are done. Then the number and positions of the catheters can be determined using a 3D rendered image with a template placed around the breast as shown in the image below. If the intention of the treatment is delivering a boost dose, steel needles can be used with 1-3fractions, but in monotherapy treatment with 7-10fractions, the needles are replaced with plastic catheters for the sake of patient's convenience.

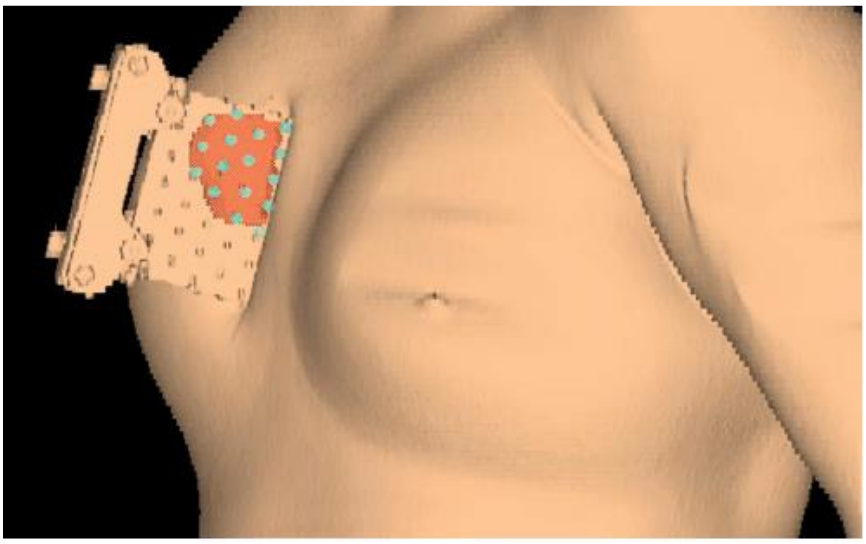

Figure 8: 3D rendering image of patient anatomy with a template on the right breast in needle's-eye-view after pre-implant computed tomography imaging. The red-colored planning target volume is projected into the template with the holes and the light-blue dots show the planned positions of the catheters[12].

Any imaging technique is used before the implantation, after the insertions of the catheters, a new CT imaging is needed for planning purpose. Generally, the patient is positioned in the CT table in the same way as for EBRT making sure the same anatomical positions at boost treatment as for external irradiation. Generally, 3mm slice thickness is acceptable for accurate catheter

reconstruction and target delineation. Organs at risk and resection cavity must be outlined, and the PTV should be created according to the available guideline. Using special markers in the catheters with good visibility but without artefact is a great help during catheter reconstruction[12]. Nevertheless, without markers, the catheters can be also visualized merely by the inside air as shown in the figure below, and with proper windowing, the reconstruction can be properly performed. Catheters should be numbered or uniquely labelled so that each individual catheter can be identified. By selecting a lower isodose level for dose prescription, the target coverage can be slightly improved, but the dose to normal tissues might increase[12].

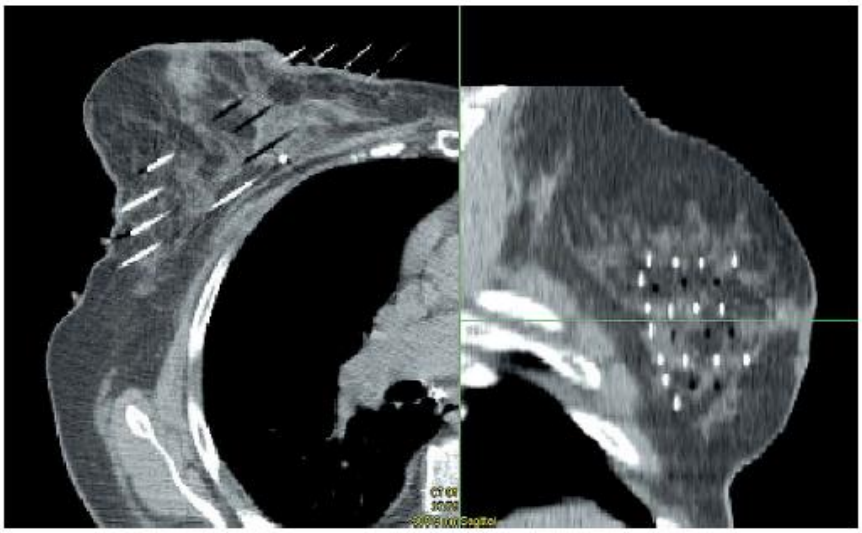

Figure 9: A transversal and sagittal computed tomography slice with implanted catheters. In most of the catheters, special markers are inserted (shown with the white lines/dots) but some of them do not have any markers and only the inside air makes them visible (shown with black lines/dots)[12].

With the introduction of image-guided implantation techniques, the treatment plans improved considerably compared to traditional fluoroscopy-guided implantation (continuous x-ray image on monitor, like x-ray movie) and planning[12]. The percentage of patients satisfied with the dosimetric goals of target coverage and dose homogeneity increased from 42% to 93%, when CT-guided technique was used instead of fluoroscopic guided free-handed catheter insertion technique[12].

2.6.2 MammoSite Balloon Brachytherapy

Balloon based brachytherapy include: MammoSite, Axxent electronic brachytherapy, and Contura [10]. MammoSite balloon brachytherapy is an approach for APBI. The MammoSite brachytherapy (MSB) system applicator was developed to be more reproducible, easily applied and better tolerated. The MammoSite catheter consists of a silicone balloon connected to a 15cm double-lumen catheter that is 6mm in diameter. The catheter has both a small inflation channel and a channel for the passage of Ir-192 HDR brachytherapy source. The source channel runs centrally through the length of the balloon. The balloon is inflated with saline solution mixed with a small amount of contrast material to aid visualization. The balloon is then inflated to a size that would completely fill the lumpectomy cavity and ensures conformance of the tissue to the balloon. An Ir-192 radioactive source connected to a computer-controlled HDR remote after-loader, is inserted through the catheter into the balloon to deliver the prescription radiation dose.

The MammoSite applicator can be placed into the lumpectomy cavity at the time of surgery or in a separate procedure after surgery. In the latter case, the applicator can be inserted under ultra-sound guidance either through the lumpectomy scar or via small separate incision. Following placement, a computed tomography (CT) scan is performed to assess the quality of the implant and for use in radiation planning. Quality of implant is determined by examination of three parameters: balloon conformance to the lumpectomy cavity, distance from the surface of the balloon to the skin surface, and the symmetry of the balloon in relationship to the central catheter. Treatment planning parameter are: the diameter of the inflated balloon, the planning target volume, and the dose distribution. While a minimum balloon-to-skin distance of 5mm is required a threshold of at least 7mm is strongly recommended. Conformance of the balloon to the lumpectomy cavity is assessed by quantifying the volume of the planning target volume (PTV) that is filled by air or seroma fluid. Adequate conformance is considered to have been achieved when less than 10% of the PTV is composed of fluid or air. A symmetric implant in relation to the source channel is also essential for adequate dosimetry. A non-symmetrical implant can result in dose inhomogeneity in the surrounding tissues since the MSB device contains a single central source channel that does not allow for shaping of the radiation isodose curves in the direction perpendicular to the central channel[10].

Figure 10: The MammoSite Balloon Applicator[12].

Recently, a Multi-lumen (4 lumen) device as seen below with the potential to eliminate some of the drawbacks of the single lumen device as in the figure above have been introduced.

Figure 11: MammoSite Multilumen System[12].

Apart from the above MammoSite systems there are several other modifications that have been designed for certain kinds of treatments or applications.

Several studies have been carried out on MammoSite balloon brachytherapy. In one study[13], results showed lower-rates of local and ipsilateral breast disease failure in a well-defined cohort of MBT patients with mature follow-up. In another study [27] which measured the extended outcomes of APBI using MBT, results showed that long-term single-institution outcomes suggest excellent tumor control, breast cosmesis, and minimal late toxicity.

2.7 Remote Afterloader and Applicators

After-loading is the technique used to deliver radiation sources. This is different from manual delivery of brachytherapy where the source is delivered into the applicator by the operator, and which is only used in few cases involving low dose rate (LDR) sources. The after-loader as indicated below by the red arrow, is a box-shaped device which passes the radiation source through a set of catheters (blue arrow) to the treatment site. It receives instruction from a control station before performing any operation. In this research, the after-loader will be used to deliver real treatment.

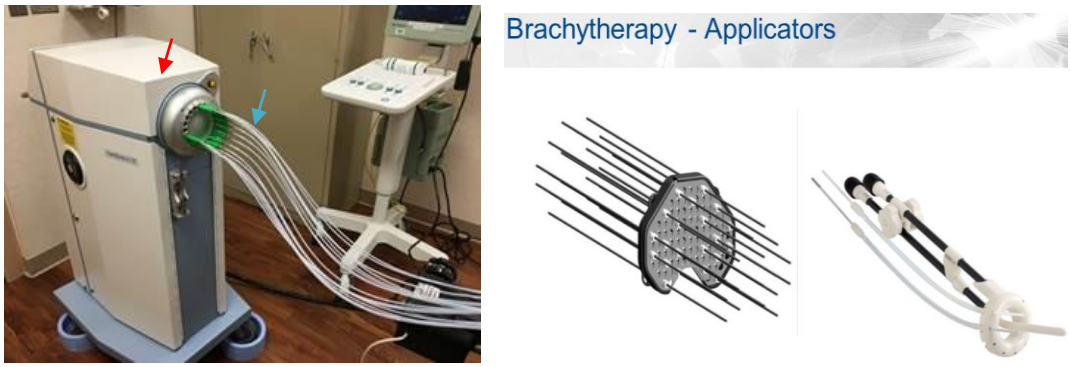

Figure 12: Afterloader, Catheter and Applicator System[17].

The applicator on the other hand is a device that comes in different designs. It is connected to the ends of the catheter, and they both provide a proper guide for the radiation source to the treatment site.

2.8 High Dose Rate Radiation Source

The main challenge in high dose rate brachytherapy (HDR) is to deliver a prescribed radiation dose to a tumor while limiting the dose delivered to surrounding organs and tissues[16]. Ir-192 is the HDR radiation source used in this research. When using the HDR source it is important that the source positions and dwell times meet the requirement for the prescribed dose. Therefore, it is particularly important to measure the real-time position and the dose distribution of the Ir-192 source in after-loading HDR brachytherapy[16]. The mean energy and half-life of Ir-192 are 370KeV and 74.2d, respectively[16].

Most HDR brachytherapy treatments are done with one weekly treatment for a period of up to four weeks or with one or two treatments per day for up to five days. The radiation delivery only lasts a few minutes while the procedure which is also called a session, including: patient setup, applicator positioning, treatment planning and treatment delivery itself, lasts up to a few hours[28].

Compared to permanent implantation, which is used to treat prostate cancer, the high dose rate afterloading therapy is used on a broader level. It can be used for the treatment of cancer in the parts of the body identified in Figure 13 below[2].

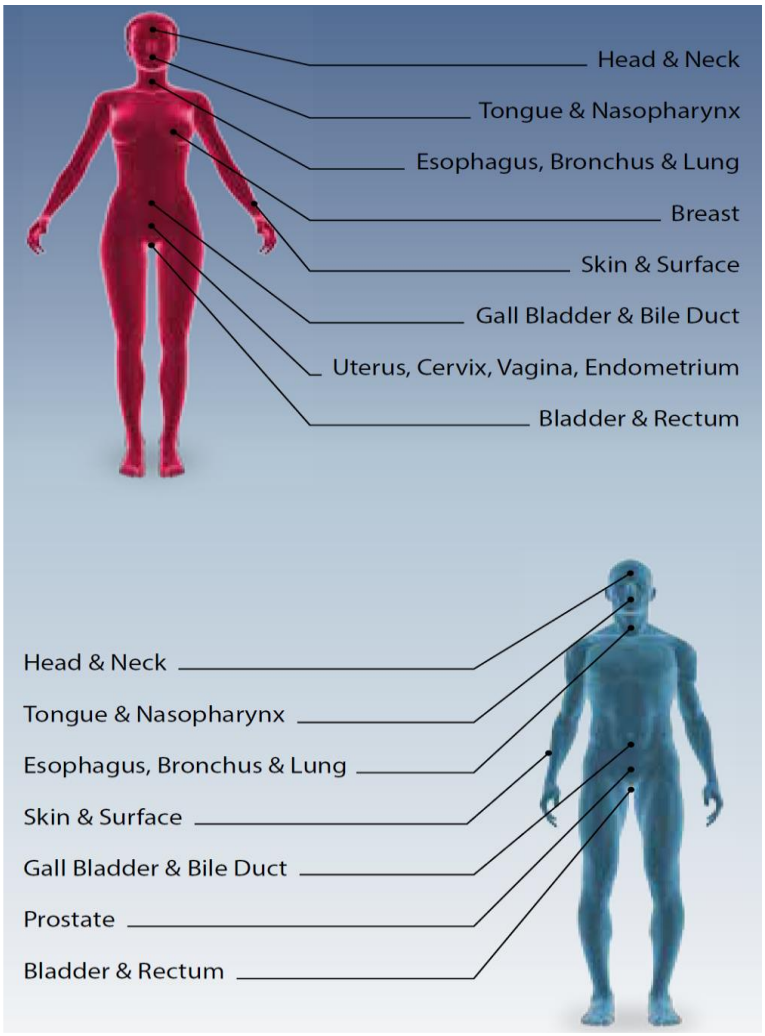

Figure 13: Body sites that can be treated with HDR brachytherapy[4].

2.9 Radiation Treatment Planning Workflow

2.9.1 Catheter Implantation

A clinical examination is performed, and several CT images of the tumor is taken for analysis. These CT images contain information including the coordinates of the region occupied by the tumor in 3D (Tumor cavity)[10,12]. The result of this analysis is used to design a treatment plan which can be delivered to the patient. Catheters are implanted either during the lumpectomy surgery or a few days later. The catheters are placed using CT-guided 3D planning software such as Pinnacle Planning Software[1]. Based on all the scans (pre-implant scans) the software outlines the cavity and creates a design for the catheter placement which includes catheter number, catheter planes, intercatheter spacing and direction of placement[1].

Figure 14: Tumor outline and planning for catheter placement[1].

Using this design, the entry-exit points for the catheters are marked on the skin of the patient 2-3 trocars are inserted in the marked points followed by the CT scan to evaluate the position of the trocar and the tumor cavity[1]. Based on the obtained information the remaining trocars are inserted and the CT scan is acquired to evaluate the accuracy of the trocar placement. Once the trocars are precisely placed they are replaced by afterloading catheters and tightly secured by buttons at both ends. Many-a-time, buttons of different colors are used to indicate different planes as a form of quality assurance procedure. The catheters are then numbered, and their lengths are recorded.

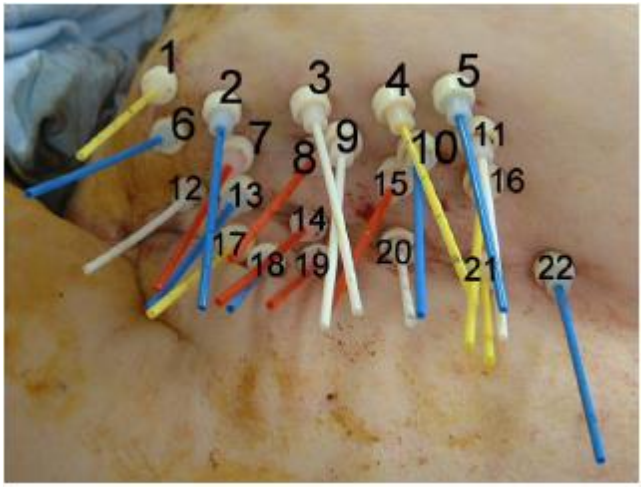

Figure 15: Catheter implant for APBI treatment[1].

After this procedure, the MammoSite device to be used in treatment is implanted using an open technique[1](during lumpectomy surgery) or using ultrasound techniques to estimate the tumor cavity (post-lumpectomy). Once the device is in place CT scans are used to evaluate the quality of the implant.

2.9.2 Creation of Phantom Patient and Plan Optimization

Since this is an experimental procedure, a phantom is initially used to validate the treatment procedure before it is applied to a real patient. A virtual or actual radiation source is used with the phantom to confirm the treatment plan (depending on preferred option). At this stage cold shots (too little irradiation) and hot spots (too much irradiation) are identified.

Measurement of the length of the catheter inserted into the phantom, is taken using a flexible circular rule which is normally inserted into the catheter to get the exact distance where the source will be placed. The source applicators are then placed in the target region (treatment area/target). Imaging techniques such as x-ray are then used to ensure correct positioning of the applicators.

2.9.3 Treatment Planning

The image dataset acquired from the procedure in 2.9.2 above is used for 3D dosimetry planning of the HDR treatment[1]. The dataset is electronically transferred to the treatment planning station. The planning station used for this research is Brachyvision Planning System, by Varian Inc. The lumpectomy cavity is then contoured along with other anatomical structures, after which treatment planning tools are used to expand the cavity by 1-2cm, keeping a 5mm distance from the chest well, pectoral muscle and the skin surface. Several factors determine this expansion such as: the size of the breast, the location and the lumpectomy cavities. The new established volume is now called the planning target volume[1].

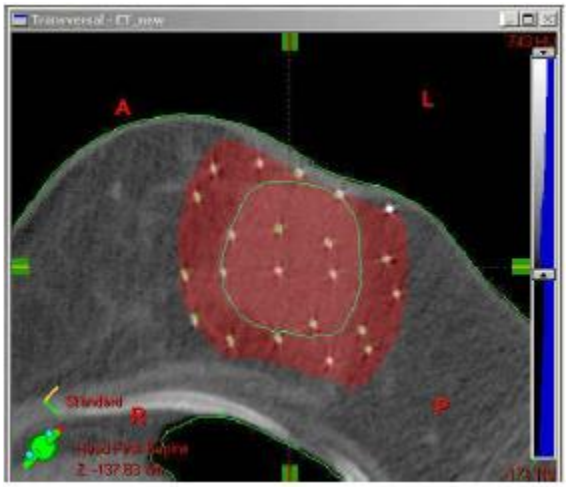

Figure 16: Contouring of tumor cavity and target volumes[1]

At this point, the applicators are outline using the 3D planning software and the CT images. The catheters are reconstructed along the dummy wire from one end of the catheter to the other. Each catheter is numbered and defined by several dwell positions.

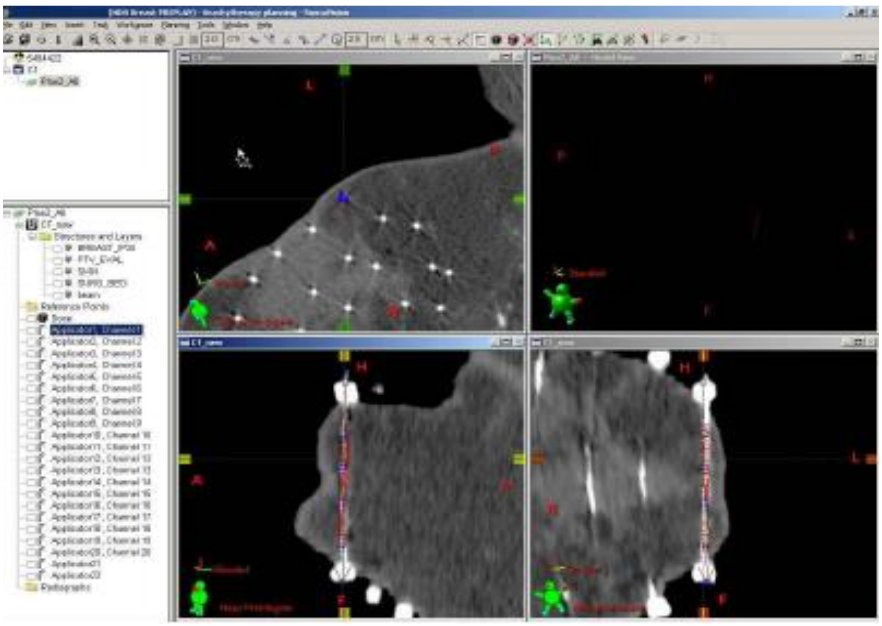

Figure 17: Explaining outlining of applicators and definition of dwell positions[1].

Next, the planning system designs a treatment plan by defining dwell times for each dwell position for all catheters target volumes. The aim of this plan is to perfectly deliver the prescribed dose to the target volumes (Dose optimization)[1].

For a well delivered plan, the dose homogeneity index should be as high as possible. Dose Homogeneity Index (DHI) is used to measure the dose homogeneity, with the formula given below[1],

$$DHI = (V100 – V150) / V100$$

V100 represents the absolute volume of tissue receiving 100% of the prescribed dose and V150 is the volume receiving 150% of the prescribed dose. The treatment plan is then evaluated using Dose-Volume Histograms.

Now that our treatment plan is ready, it is exported to the computer station used to control the afterloader. This plan contains all the dwell positions with their accurate dwell times, for each applicator. The catheter lengths are added to the appropriate applicator and fed to the treatment delivery system. The Ir-192 radioactive source of 34Gy[1] is used for treatment, via the afterloader, in a selected number of fractions over several days.

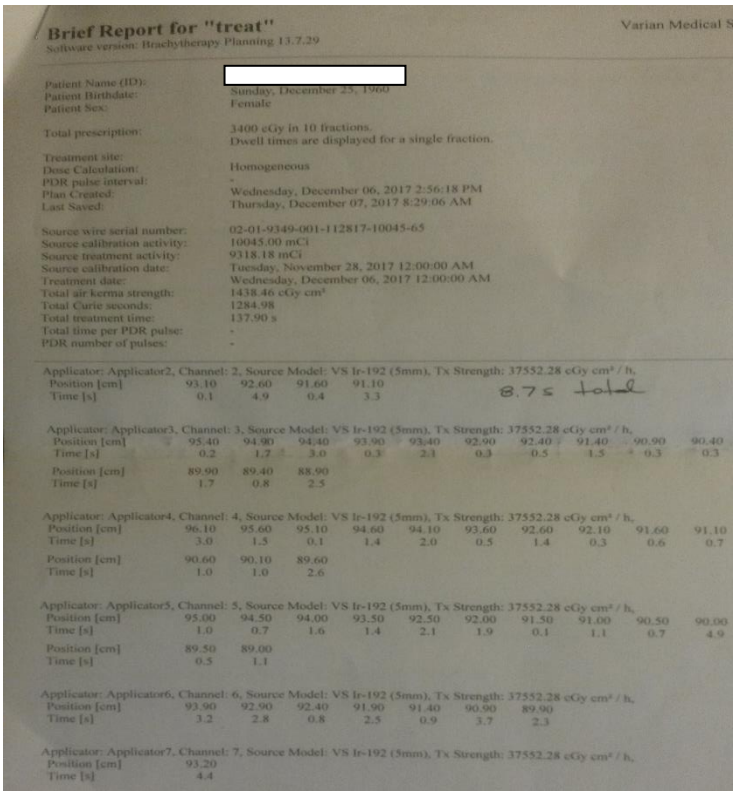

Brief Report for "treat"
Software version: Brachytherapy Planning 13.7.29
Varian Medical S

Patient Name (ID): [redacted]
Patient Birthdate: Sunday, December 25, 1960
Patient Sex: Female

Total prescription: 3400 cGy in 10 fractions.
Dwell times are displayed for a single fraction.

Treatment site:
Dose Calculation: Homogeneous
PDR pulse interval: -
Plan Created: Wednesday, December 06, 2017 2:56:18 PM
Last Saved: Thursday, December 07, 2017 8:29:06 AM

Source wire serial number: 02-01-9349-001-112817-10045-65
Source calibration activity: 10045.00 mCi
Source treatment activity: 9318.18 mCi
Source calibration date: Tuesday, November 28, 2017 12:00:00 AM
Treatment date: Wednesday, December 06, 2017 12:00:00 AM
Total air kerma strength: 1438.46 cGy cm²
Total Curie seconds: 1284.98
Total treatment time: 137.90 s
Total time per PDR pulse: -
PDR number of pulses: -

Applicator: Applicator2, Channel: 2, Source Model: VS Ir-192 (5mm), Tx Strength: 37552.28 cGy cm² / h,
Position [cm] 93.10 92.60 91.60 91.10
Time [s] 0.1 4.9 0.4 3.3
8.7 s total

Applicator: Applicator3, Channel: 3, Source Model: VS Ir-192 (5mm), Tx Strength: 37552.28 cGy cm² / h,
Position [cm] 95.40 94.90 94.40 93.90 93.40 92.90 92.40 91.40 90.90 90.40
Time [s] 0.2 1.7 3.0 0.3 2.1 0.3 0.5 1.5 0.3 0.3
Position [cm] 89.90 89.40 88.90
Time [s] 1.7 0.8 2.5

Applicator: Applicator4, Channel: 4, Source Model: VS Ir-192 (5mm), Tx Strength: 37552.28 cGy cm² / h,
Position [cm] 96.10 95.60 95.10 94.60 94.10 93.60 92.60 92.10 91.60 91.10
Time [s] 3.0 1.5 0.1 1.4 2.0 0.5 1.4 0.3 0.6 0.7
Position [cm] 90.60 90.10 89.60
Time [s] 1.0 1.0 2.6

Applicator: Applicator5, Channel: 5, Source Model: VS Ir-192 (5mm), Tx Strength: 37552.28 cGy cm² / h,
Position [cm] 95.00 94.50 94.00 93.50 92.50 92.00 91.50 91.00 90.50 90.00
Time [s] 1.0 0.7 1.6 1.4 2.1 1.9 0.1 1.1 0.7 4.9
Position [cm] 89.50 89.00
Time [s] 0.5 1.1

Applicator: Applicator6, Channel: 6, Source Model: VS Ir-192 (5mm), Tx Strength: 37552.28 cGy cm² / h,
Position [cm] 93.90 92.90 92.40 91.90 91.40 90.90 89.90
Time [s] 3.2 2.8 0.8 2.5 0.9 3.7 2.3

Applicator: Applicator7, Channel: 7, Source Model: VS Ir-192 (5mm), Tx Strength: 37552.28 cGy cm² / h,
Position [cm] 93.20
Time [s] 4.4

Figure 18: Sample Treatment plan

2.9.4 Software

Most of the software used in this research comprises of MATLAB codes. Communication with the flat panel detector will require the use of Embedded C code which will be integrated with MATLAB via MATLAB Exchange Files(MEX), such that the entire setup can be controlled via the MATLAB GUI. The software used by the actual treatment system is separate from that which we design in this research. Ours is meant to work alongside the main treatment system, and act as a standalone monitoring system.

Now that we have an overview of the actual structure of our software, it is important to note that certain modifications had to be made to get all our codes running properly. Figure 19, below shows the location of the sample codes created, on the computer when the software that comes along with the flat panel detector is installed. The software only works on Windows 7, and I believe the same thing applies to the driver that ensures communication between the detector and the software. Since we intend to control our system from MATLAB, we must create a custom design using the sample embedded C-program provided to us. For optimal performance this code had to be modified to reduce its total size and runtime. The reduced/modified code is then

packaged as a MEX file to make it compatible with MATLAB. This MEX file along with the image processing algorithms and other native MATLAB codes that are designed to extract information from the DICOM files, are made to all run together for our design to properly function.

To ensure optimal performance, our image detector has to have a high/fast read-out time, and our MATLAB image processing algorithms need to run at very high speed to reduce delay, and to ensure that we get results almost in real-time, if not in realtime[17].

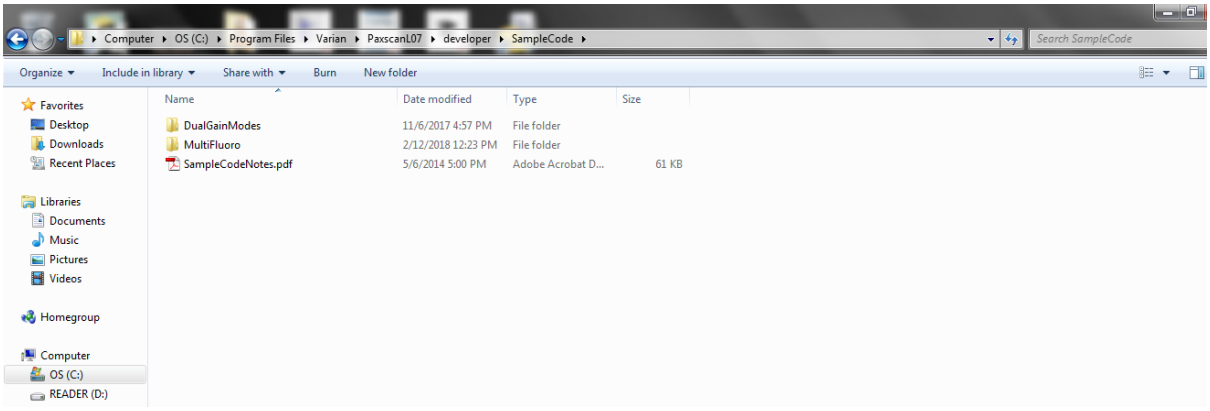

Figure 19: Shows location of sample C codes after installation of Varian software

Communication with the flat panel detector is done over ethernet. As recommended by the manufacturers communication is done over this IP address: 192.168.2.23. The figures below show how we navigated to and set the IP on the computer to make this work.

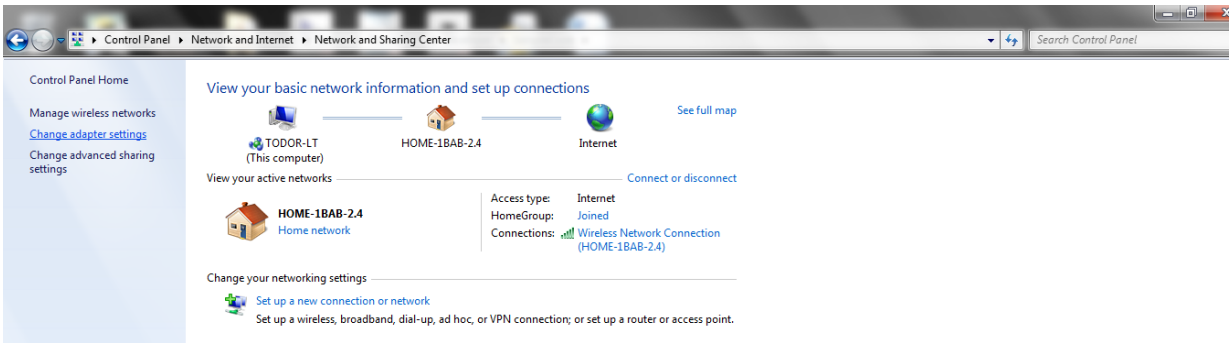

Figure 20: First step to modify Ethernet IP of the flat panel detector

Figure 21: Second step to modify ethernet IP of the flat panel detector

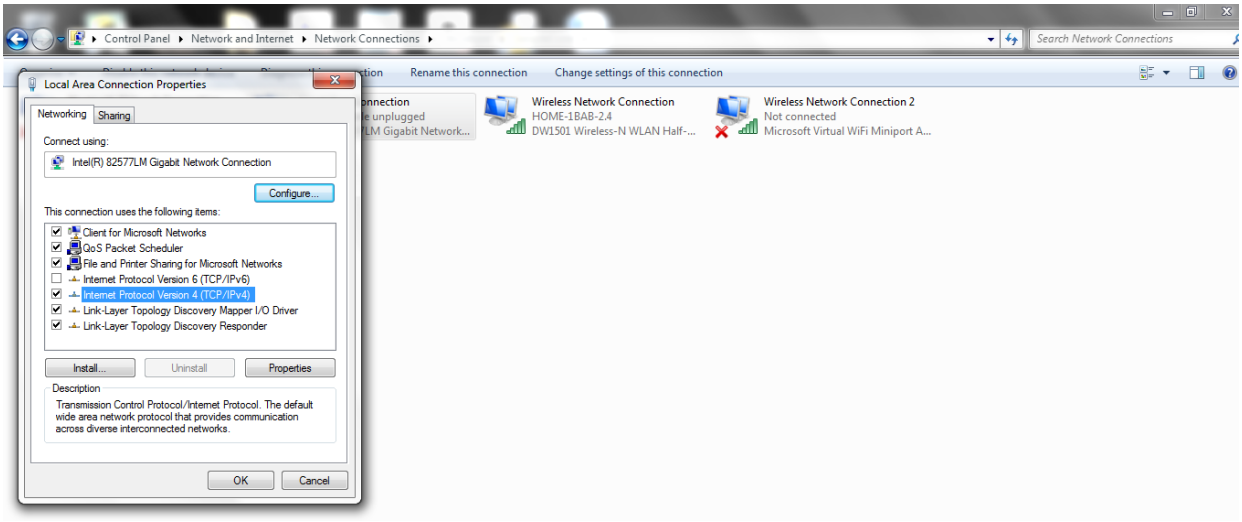

Figure 22: Third step to modify ethernet IP of the flat panel detector

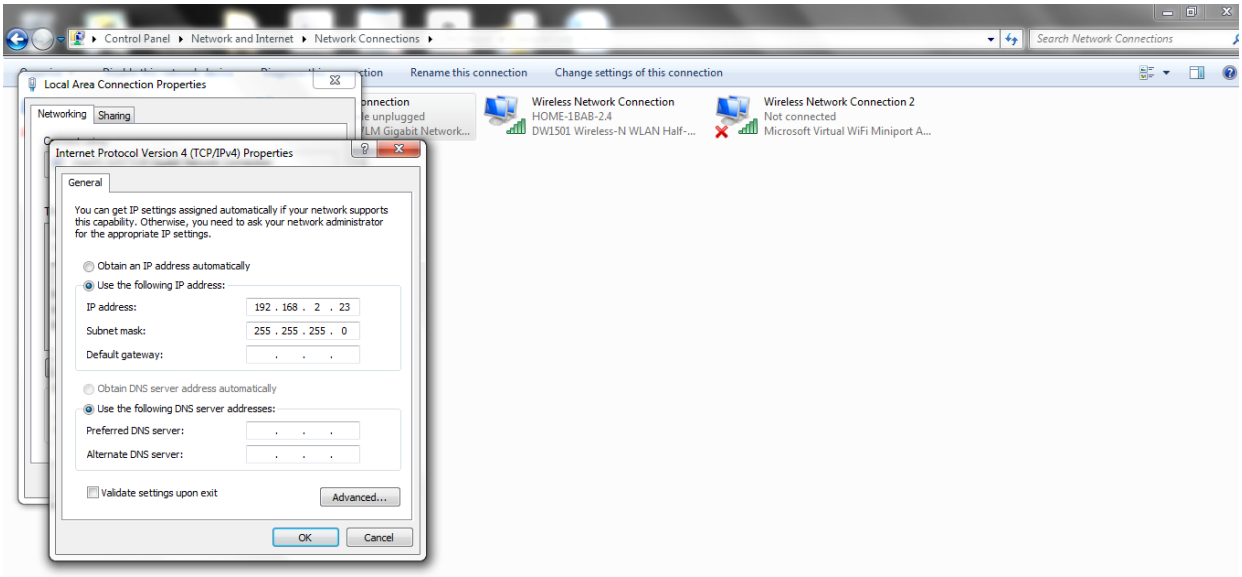

Figure 23: Fourth step to modify ethernet IP of the flat panel detector

2.9.5 Quality Assurance (QA) Procedures:

Factors resulting in dosimetry errors which potentially affect the efficacy of treatment includes: anatomical changes between the time of planning and surgery, human error in measuring and entering data to the after-loader system, and changes in the catheter location during the treatment or from fraction or fraction.

Quality Assurance is a major factor in brachytherapy; physicians are usually encouraged to make the best use of radioactive treatment materials to protect healthy tissues in the patient as well as protect the environment, as per regulations set by the nuclear regulatory commission (NRC)[19].

It is doubtful that the use of radionuclides for brachytherapy can be replaced in the near term by some non-radionuclide equivalent source of radiation. Doctors see it as superior to external radiation, since it causes the least damage to surround tissue. X-ray units are simply too large as well for internal use and there is no current adequate alternative to the use of radionuclides in brachytherapy[20].

In some parts of the world, total safety is a serious concern; for example, in Canada, where a National Sealed Source Registry (NSSR) and the Sealed Source Tracking System (SSTS), were developed. These systems contain information on the movement and location of high-risk radioactive sources in Canada, from their manufacture to their final disposition (cradle-to-grave approach)[21].

CHAPTER 3 METHODOLOGY

This experiment was setup in the basement of the North hospital in VCU Massey cancer center, in the brachytherapy imaging suite located in the basement. The HDR source tracking setup comprised of the: imaging source, a well-defined array of markers and a detector. The HDR source (from the after-loader) was used for all imaging purposes. The flat panel detector used here is of higher sensitivity as compared to the one used in the previous research [1]; it was used as the image detector for all the test runs. For image acquisition purposes, ball bearings (BBs) of 4mm to 6mm in diameter purchased from Pleasants Hardware and a local bicycle shop were used to create the array of markers.

As shown in Figure 24 below, the basic experimental setup has the HDR source positioned at some distance away from the detector, with the set of markers placed at some distance between the source and the detector. In Figure 24 we have two planes namely: the marker plane and the detector plane. The surface of the new flat panel detector makes up the detector plane while the top surface of the plexiglass makes up the marker plane. Assume P1 and P2 in Figure 24, represents two markers placed at some random position on the plexiglass. The system of axis for this experiment was chosen such that the center of the detector acts as the origin, with the x-axis and y-axis running through the center of the detector and the z-axis perpendicular to the center of the detector. This system made calculation convenient. A single test applicator with five dwell positions placed along the x-axis was used for all our experiments.

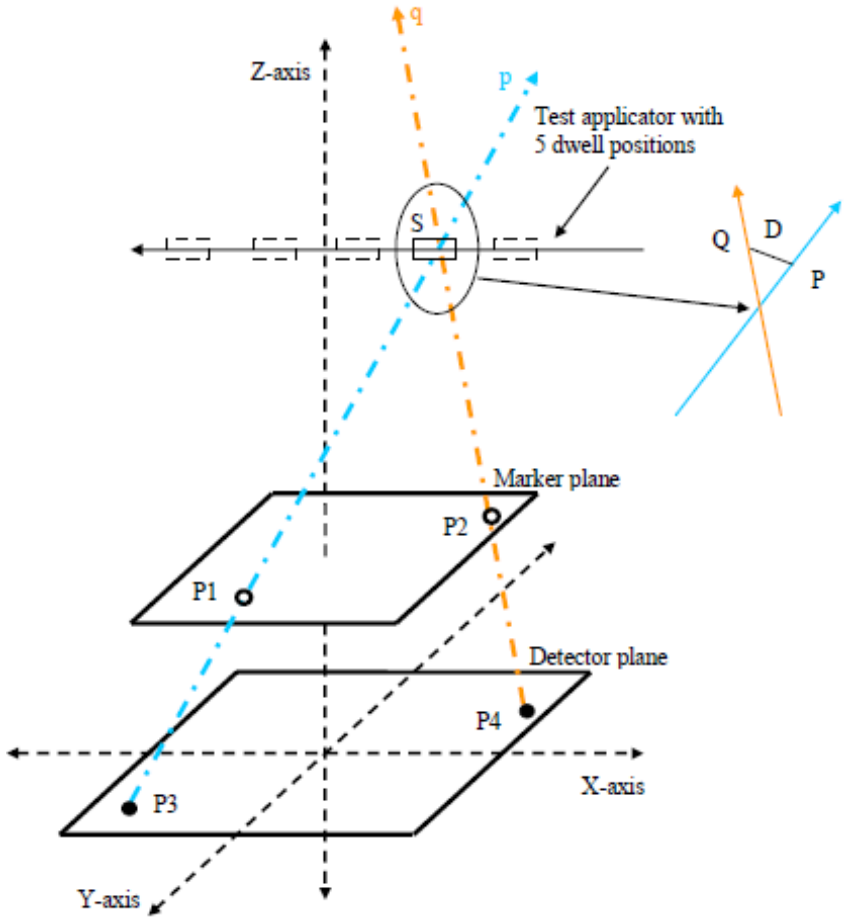

Figure 24: Schematic of the experiment

Take point S as one of the dwell positions where the HDR source will be active for a set amount of time. When the HDR source reaches point S and is active, it will produce projections of the various markers (BBs) on the detector; marker P1 produces projection P3 and marker P2 produces projection P4. To define a line in 3-D which passes through the marker and its projection we need to know the coordinates of the markers and its projections with respect to the origin in space. Line p is defined by the combination of marker P1 and its projection P3, while line q is defined by the combination of marker P2 and its projection P4. The intersection of imaginary line p and q in 3-D space constitutes the original position of the source S. This procedure is repeated to track the other dwell positions.

Since two non-parallel lines don't necessarily intersect in space, as they could go over one another without touching, we might not have any point as common points. Thus, plotting the true intersection of line p and line q in space is very unlikely. To resolve this, we compute the shortest distance between two lines, by connecting them in 3D using a line segment which is perpendicular to both lines. The shortest of such line segment is unique and is considered as the

intersection of the two lines in 3D. This distance is represented by D, and it's the shortest distance between line p and line q, while P and Q represent the corresponding two points contained on line p and line that make up D. The mean of the coordinates of point P and Q would give us the 3-D coordinates of the source position.

The explanation above uses just a pair of markers; in this study a well define matrix of markers is used. The procedure above is repeated for all possible combination of marker projection pairs. N markers would produce N*(N-1) / 2 combination of marker projection pairs. Each pair will produce a shortest distance D, a P and a Q. The average over all the P's and Q's will give the most accurate position of the source.

3.1 DICOM Files

Digital Imaging and Communications in Medicine (DICOM) is a standard for storing and transmitting medical images enabling the integration of medical imaging devices such as scanners, servers, workstations, printers, network hardware, and picture archiving and communication systems (PACS) from multiple manufacturers[15]. It describes how to compose messages to send between imaging modalities (example: CT, MRI) and defines a set of operations for transmitting them across a network. These messages can also be written to files for offline storage on a picture archiving system, CD, or other type of storage device. DICOM-formatted messages combine images and metadata to create a rich description of a medical imaging procedure. This format is extremely detailed, with a specification that is more than 2500 pages long[15].

A typical DICOM file contains numerous attributes or metadata. The reason for this is that DICOM message encapsulate all the information about medical imaging procedure, including details about the patient, study, imaging modality, and image series in addition to the image frame stored in the file. Together, all these attributes comprise an information object.

DICOM makes it easy to acquire and put medical images into a file. It is becoming more prevalent in the medical field. Many medical device manufacturers and software manufacturers are adding DICOM to just about any product that can work with medical images and data.

Using MATLAB with the image processing toolbox provides easy access to medical images, modality, metadata, and patient information within DICOM files. They also provide numerical and image processing algorithms, GUI-building tools and visualization techniques. With MATLAB, the image processing toolbox and DICOM we can view medical images, design and test new modalities, and create GUI-driven medical image analysis systems.

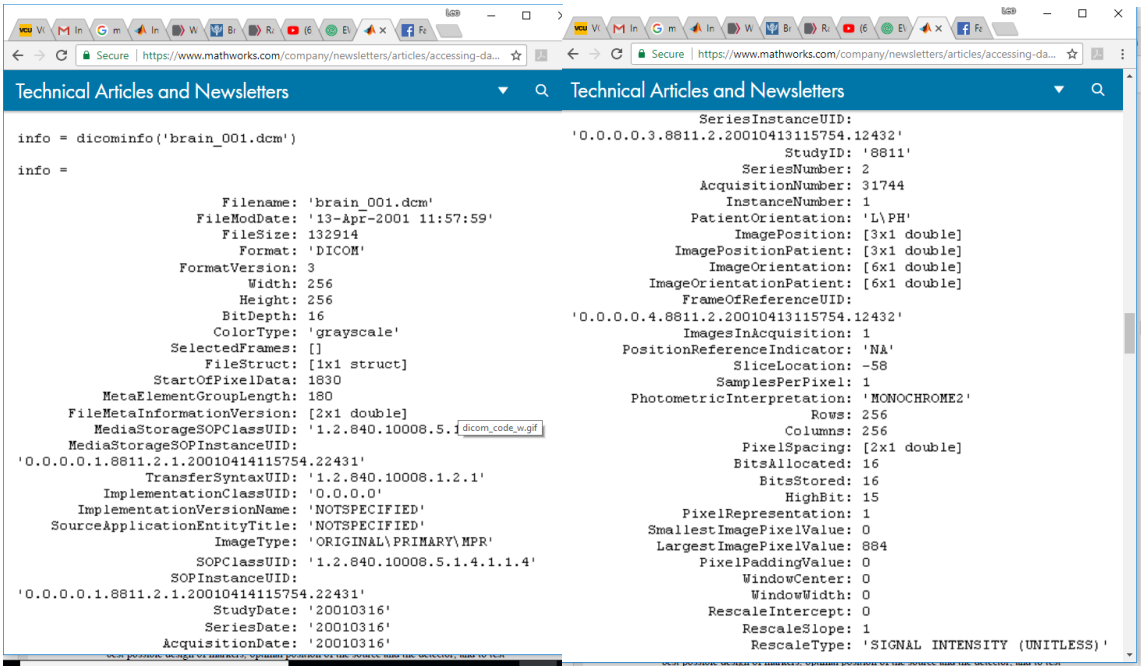

Figure 25: Sample DICOM metadata[15].

The DICOM file used here holds several groups of data of different datatypes (metadata). These groups are called fields and could contain sub-groups of various datatypes as well. It basically has a tree structure, which opens as you go deeper into it, just like a folder or directory. Figure 26, below show the content of the DICOM plan file (struct file) read into a variable named "infop" in MATLAB. It is of struct datatype.

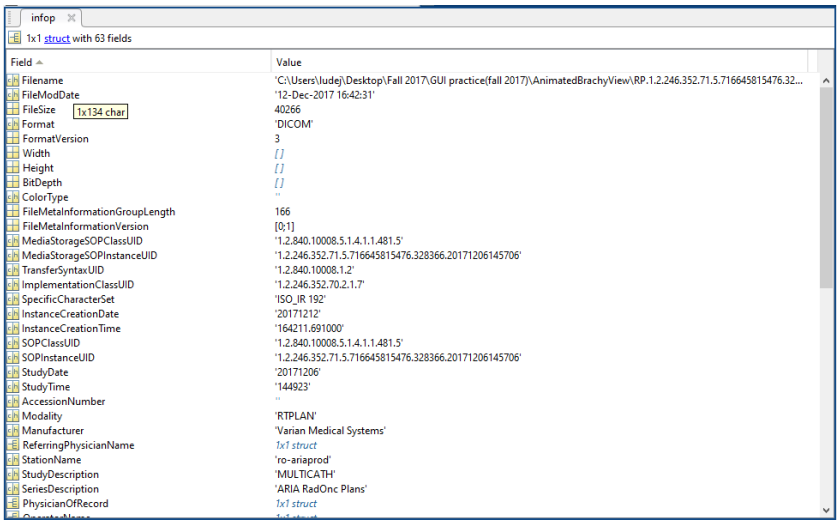

Figure 26: Sample Content of a DICOM file

3.2 Testing Imaging Geometry and Image Quality

The radiation produced by the HDR source must be strong enough to be used as an imaging source. In other to resolve the problem of image quality when using a given HDR source, the new Varian detector has a higher sensitivity. The flat panel detector (FPD) is optimized for the low energy of the X-ray imaging source (80 – 120kV range). The average energy of Ir-192 source used for HDR treatments is approximately 380KeV, well outside of the range for which the FPD is optimized. Given a likely distance of 0.5m-1.0m between the radioactive treatment source Ir-192, and the FPD, the intensity of the beam is going to be significantly less than that of the X-ray source, which will translate in low signal to noise ratios (S/N ratios).

The aim of this test is to define the best imaging geometry for the experiment: the best possible design of markers, optimal position of the source and the detector, and to test image quality. A good projection of markers produced by the HDR source for different source-detector distance can be isolated and labeled.

A good imaging geometry would also include a well-defined matrix of markers and an optimal height between the markers and the detector, such that every marker of the matrix produces a projection on the detector. The concept of estimating optimal height is really finding the best compromise between large image displace and good image quality. Let's assume the source moves from position S1 to position S2 as in Figure 27, when the markers are placed away from the source and closer to the detector the resulting scatter will be significantly less, thus producing good quality images. But the displacement of the marker projection on the flat panel detector for a given source displacement would be very small relative to the detectors resolution that is 0.388mm. When the markers are placed closer to the source and away from the detector, although the displacement of the projection of the markers would be larger, larger amounts of scatter would deteriorate the quality of the image.

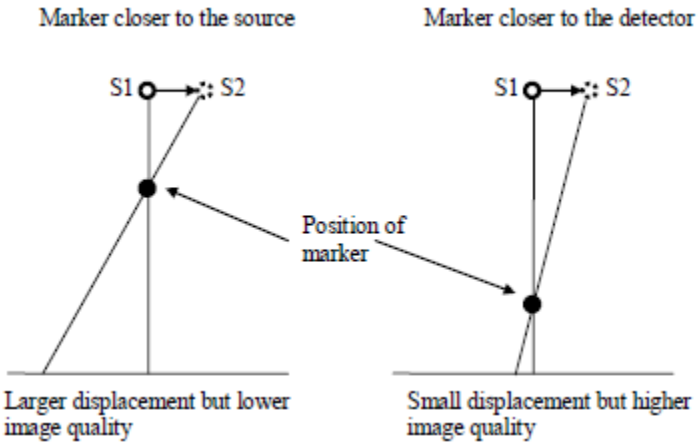

Figure 27: Explaining position of markers for a good imaging geometry

On average a breast cancer tumor is less than a 15cm × 10cm × 10cm cube. Thus, for the calculations we assumed that the source would travel a maximum of 15cm in the x-axis, and 10cm in the y-axis within the tumor. The dimension of the detector is 40cm × 30cm. A region must be defined such that when the matrix of markers is placed within that region, every single marker in the matrix would produce a projection on the detector.

Looking at Figure 28, let's assume the source-detector distance is 60cm, and assume that line AB represents the 15cm side of the cube that the source is supposed to travel within the tumor, and line PQ represents one side of the detector.

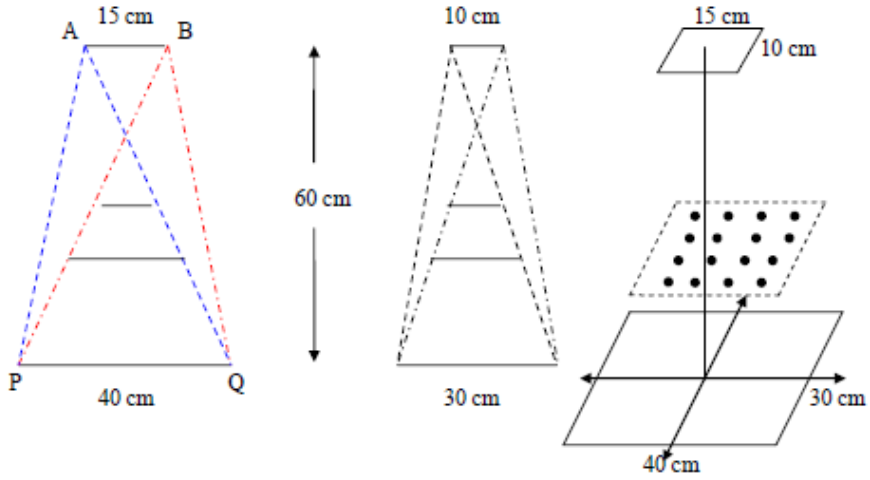

Figure 28: Explaining the region of interest for the position of the markers[1].

When the source is at point A, all markers within the area covered by the blue dotted lines will produce projections on the detector. Now when the source is at point B all markers with the area covered by red dotted lines will produce projections on the detector. The intersection of these two areas or regions represents our region of interest. Within this area of interest, we need to find an optimal height where there is no compromise on image quality or distance of image displacement. At the same time, it must give room for decent amount marker projections to be produced on the detector. Looking at Figure 28 above it was discovered that 20cm to 30cm is a good height to place a set of markers such that all projections fall on the detector[1].

Once the range of distance between the marker and the detector has been defined, the next step is to design the basic experiment by placing the Plexiglas detector setup and acquire images using the HDR source. Markers with different diameters were placed 1cm to 2cm apart on top of the plexiglass surface. The markers were placed along the two-central axis of the detector. The source-detector distance was varied from 40cm-70cm with an increment of 5cm, keeping the

distance between the markers and the detector constant at approximately 20cm. Images were acquired using the HDR source and the flat panel detector.

The activity of the HDR source will produce projections of the markers on the flat panel detector and these can be captured on the detector from the control area by activating the start tracking process using a MATLAB GUI from the control area. The images obtained are named and saved in a specified directory in the remote computer controlling the image detector (control area). These images are then converted to DICOM format via MATLAB code and are processed by MATLAB.

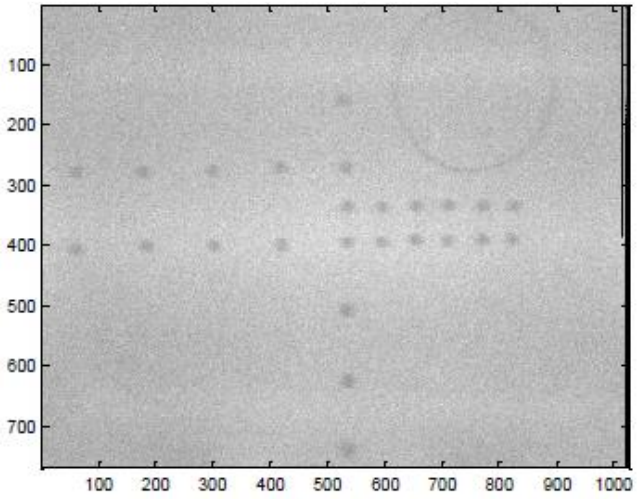

Figure 29: Grey scale image acquired using the HDR source and flat panel detector with source-detector distance of 50cm to check imaging geometry and quality

Figure 29 shows a gray scale image of the projection of marker when the source-detector distance was 50cm[1]. In the previous research, the best quality images were produced when the source-detector distance was at 50cm and when the markers were spaced 2cm apart. The images were taken to check image quality; they proved that the marker could easily be seen by eye. The best quality images were produced when the source-detector distance was at 50cm and when the markers were spaced 2cm apart.

Now that we have our image the next step was to segment out only the markers, label them and get their centroids. The centroid would then be used as a surrogate for the coordinates for the

projection of the markers. Using MATLAB the raw images saved in DICOM format could be read using the dicomread command as explained below:

```
Info = dicominfo(FileName);

X=dicomread(info);
```

“dicominfo” reads the metadata from the DICOM file specified by the string “FileName” and store it in the variable info. “dicomread” then reads the image data from the DICOM metadata structure “info” and stores it in variable X.

The image data contains ample information including, coordinates of the marker, patient information, applicator coordinates, projection of the markers, random noise etc. Image averaging and noise filters were used to remove the noise. Once a smoother grayscale image with minor grains is obtained, the aim was to segment out only the markers and leave out the noise. Given that the shape of the markers was known before hand, morphological operations is used to localize and segment the marker. A threshold is applied to convert the grayscale image to a binary image in which the markers are represented by ones and the rest by zeros (image processing explained later in the chapter). From the binary image the markers could be easily segmented, labeled and their centroids could be calculated.

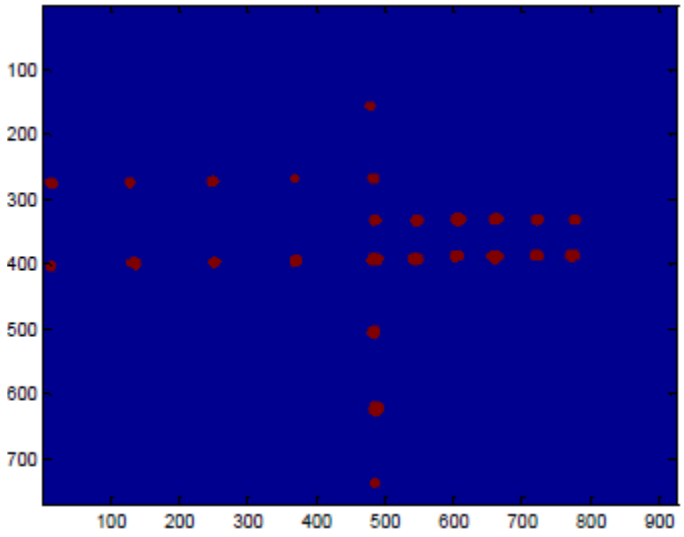

Figure 30: Binary image obtained after morphologically processing and segmenting the grayscale image.

3.3 MEX Files

MEX stands for MATLAB executable. It is a type of computer file that provides an interface between MATLAB or Octave and functions written in C, C++ or Fortran. When ran, they are dynamically loaded and allow external functions to be triggered from MATLAB or Octave as though they were built-in functions[25].

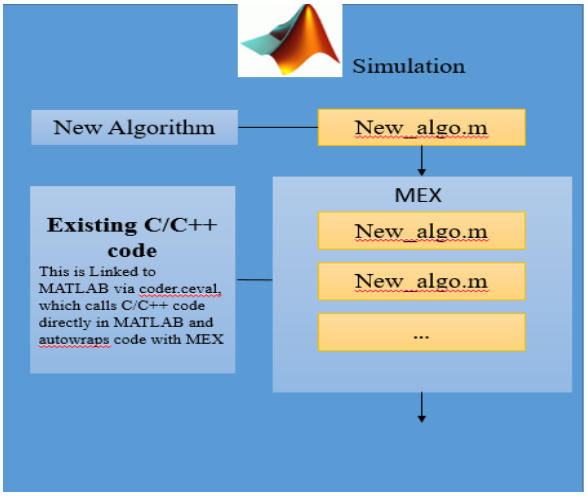

Figure 31: MEX file structure

3.4 Experimental Setup

The brachytherapy imaging suite at Virginia Commonwealth University is equipped with Acuity which is an imaging and simulation machine manufactured by Varian Medical System, Inc. For the experimental setup we used the: the flat panel detector setup, the after-loader, guide tubes(catheter), a 5cm solid water phantom, test catheter and the operating couch.

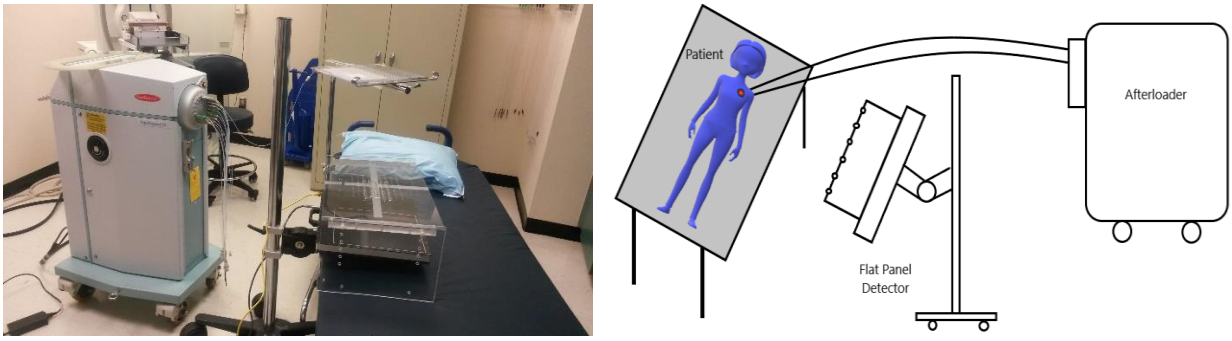

Figure 32: Representation of the experimental setup

The detector used in this experiment is a new highly sensitive flat panel detector from Varex Imaging which is a branch of Varian Medical Systems Inc. The flat panel detector setup has an arm that attaches it firmly to a stand. The arm can be moved through several angles to acquire images. The total pixel area of the detector is approximately 40cm(h) × 30cm(w), with a total pixel matrix of 1088(h) × 896(w) at half resolution and 2176(h) × 1792(w) at full resolution. For all the experiments the detector was used at full resolution, contrary to the previous work[1], and with a pixel size of 0.0388cm.

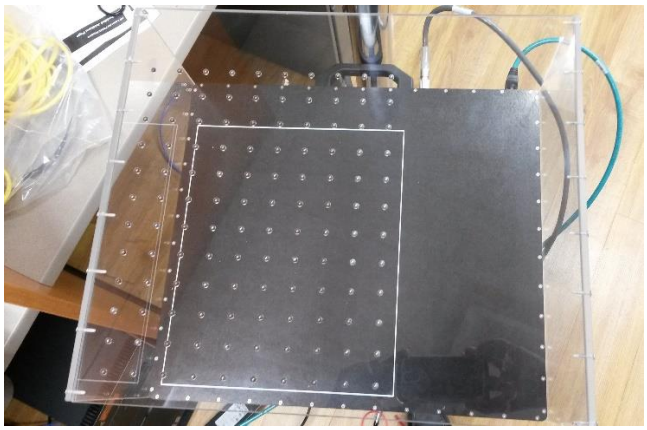

Figure 33: Arrangement of matrix of markers

A mount was made from Plexiglass to hold the markers at a fixed height above the detector. The plexiglass was permanently mounted atop the flat panel detector with the help of screws. Adjustable screws are also made available to control the height of the mount. The markers are

arranged in the form of a well-defined matrix. Figure 33 shows a well-defined arrangement of markers above the detector's receptor area.

Iridium 192 was the HDR source, it was stored and delivered via the after-loader present in the suite. The after-loader used was VariSource iX, bu Varian medical systems Inc. The after-loader serves as a storage location for the HDR source; it can shield the environment from the source. The HDR source is normally present at the tip of a source in the after-loader; this way it could be delivered and retracted into the after-loader from a remote operating console for safety reasons. The remote operating console uses a source control and drives mechanism to sort, control and move the source into specific positions for a specified amount of time. The after-loader has twenty output channels, with guided tubes connected to each output. The HDR source can be delivered via any of the twenty output channels. The guide tubes are long rubber catheters which connect one of the output channels of the after-loader to the test catheter.

The test catheter used for this experiment is made of plexiglass. It has a thickness of 0.6cm. The plexiglass sheet contained horizontal cylindrical holes of 0.5cm in diameter which were sealed from one side and open from the other. The test catheter was placed inside these holes with some part of the catheter left outside the plexiglass. The guided tubes were clipped on to the part of the catheter left outside the plexiglass, thus creating connection between the after-loader and the test catheter.

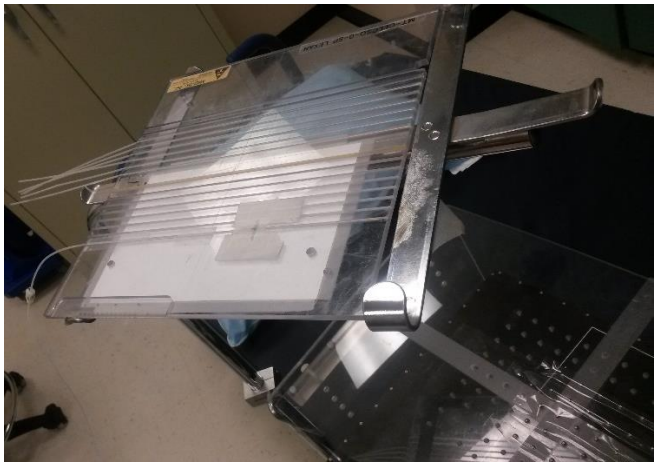

Figure 34: Test Catheter with flat-panel-detector-set positioned below it

A 5cm solid water phantom was used to mimic the patient. The test catheter was place on top of the solid water and this arrangement was placed on the operating coach to portray an actual treatment scenario. The after-loader delivers the HDR source through the guided tubes to a position in the test catheter and holds the source in that position for a given amount of time.

3.5 Calibrating the System

This process comprises two steps. Firstly, the exact height between the marker plane and the detector plane is calculated. Next, we calculate the coordinates of the position of the markers with respect to the origin. Since the actual surface of the detector (image sensor) is packaged within the cover of the flat panel detector, the height between the markers and the detector cannot be manually measured, accurately. The Plexiglass mount used to place the markers is currently stably mounted. An x-ray source placed at a known height was used to acquire images for calibration.

3.5.1 Calculate Height: To calculate the coordinates of the markers on the marker plane, the exact height between the two planes must be known. Figure below represents the image acquired using the x-ray source. It is a grey scale calibration image and the red dotted line represents the central axes.

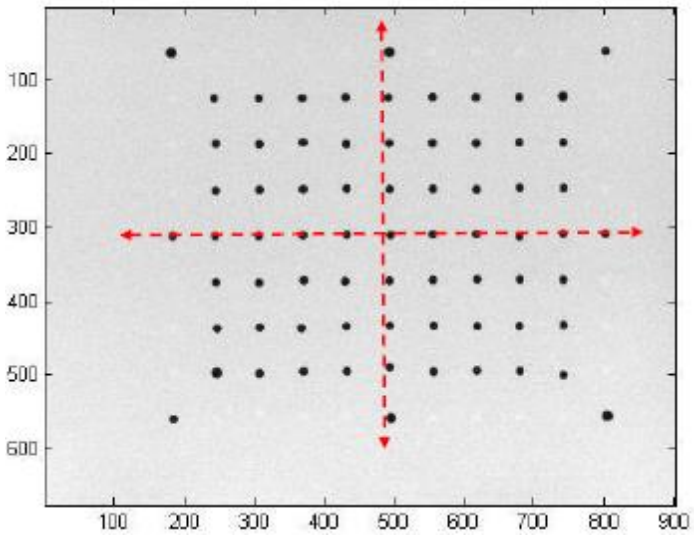

Figure 35: Grey scale calibration image[1]

The markers are arranged such that there exists an array of markers along the x-axis and y-axis. The markers on the central axis are used to calculate the height between the two planes. From Figure 35, a marker exists on the axis of the origin. Using this marker as a reference, we can calculate the distances to other markers and projections along the x-axis and y-axis. Morphological image processing is applied on raw images to segment and label them, after

which the centroid of the projections of the markers is calculated. This way we can get the distances between the projections of the markers. Using these distances, we can calculate the height H using the formula below.

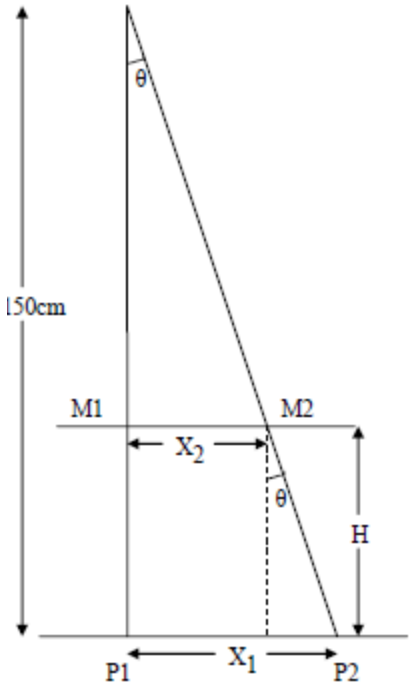

Figure 36: Schematic representation of height calculation[1].

Assuming M1 is the marker on the same axis as the origin, with its projection as P1, and M2 is the represents any other marker along the x-axis or the y-axis with P2 as its projection. This x-ray source is kept at a fixed distance from the detector which can be electronically controlled from the operating console. For the first and second trial this distance was fixed at 150cm[1], and for the third trial it was fixed at 170cm[1]. H represents the height between the markers from the detector, X_2 represents the distance between the markers on the marker plane and X_1 represents the distance between the projections of the markers on the detector plane.

The coordinates of the centroid in the segmented image represents the pixel. This can be converted to centimeters by simply multiplying it with the resolution of the flat panel detector, 0.0388cm. Once the coordinates are converted to centimeters X_1 is calculated by subtracting the

coordinates of the markers along the x and y axis from the origin. X_2 is manually calculated using a foot ruler.

Looking at Figure 36, Tanθ can be represented by two equations

$$\text{Tan}\theta = X_2 / (150 - H)$$

$$\text{Tan}\theta = (X_1 - X_2) / H$$

The formulas above, produces the formula below when solved simultaneously.

$$H = 150*(X_1 - X_2) / X_1$$

The above formula will give the value of H for one marker with respect to the central marker. This same procedure is repeated to calculate the distances between all the markers and its projections with respect to a selected origin. Using the distance H is calculated for the respective markers and a mean of all the H's is used as the height between the marker plane and the detector plane.

This procedure was used for the first two trials. The third trial had the x-ray source placed at 170cm from the detector[1]. Every other procedure remains the same, except the formula for the calculation of H:

$$H = 170*(X_1 - X_2)/X_1$$

3.5.2 Calculate the Coordinates of the Markers: The unprocessed detector image used to calculate the height is also used to calculate the coordinates of the markers. The origin is assumed to be the center of the detector for all coordinate calculation purposes. For calibration purposes the x-ray source is placed along the z-axis at a height of 150cm, so that the x-ray source has the coordinate of [0, 0, 150]. The height at which the markers are placed represents the z-coordinates of the markers with the x and y coordinates unknown, i.e. [x, y, H]. H is calculated using the formula for H. The aim here is to calculate the x and y coordinates of the markers using the coordinates of the projection of the markers on the detector.

The steps taken to get some much-needed coordinates are as follows: first the image is acquired, then it is processed so that it can be segmented and labeled. The centroid for each of the labeled marker is then calculated with respect to the origin. The coordinates of the centroid are converted to centimeters using the resolution of the detector. Once the coordinates of the x-ray source, the projection of the markers and the z-coordinate of the markers are known, the 3-D coordinates of the markers can be calculated using the equation of the line in space. These processes were

accomplished using a custom written algorithm implemented using MATLAB and the image processing toolbox.

Figure 37 shows the x-ray source placed at point S[0, 0, 150], two random markers used for calibration C1 and C2 and their projections C3 and C4. From the figure we observe that S, C1 and C3 form a straight line in 3-D.

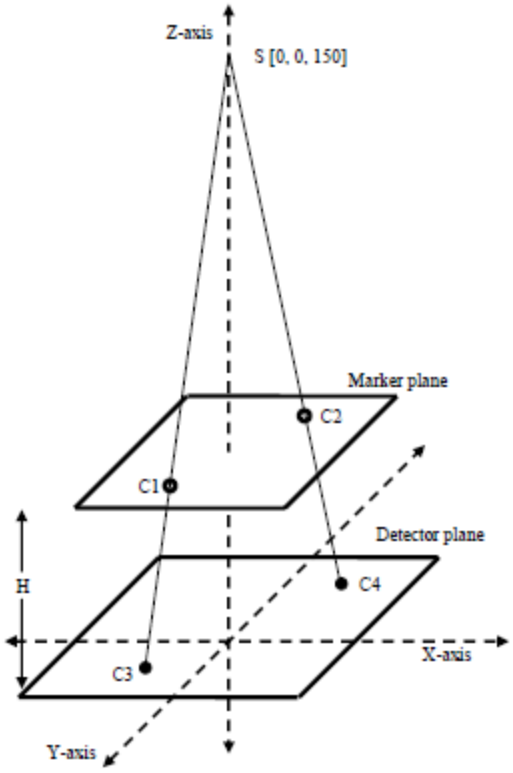

Figure 37: Represents a schematic for calculating the coordinates of the markers from the calibration image[1].

The line can be represented by the three parametric equations:

$$X = x1 + t(x2-x1)$$

$$Y=y1+t(y2-y1)$$

$$Z=z1+t(z2-z1)$$

Where t varies from $-\infty$ to ∞

The 3D coordinates of the source S and point C3 are known. The z-coordinate for point C1 is also known[1]. Substituting the values of the z-coordinates in the equation for Z we get t = H/150. By substituting the value for t and the values for x and y coordinate of the source and the projections in the equations of X and Y, the 3-D coordinates of the markers with respect to the origin is calculated.

3.6 Test Plans

A plan gotten from CT and stored in a database as shown in Figure 38, below is used in this treatment. The plan comes in the form of a DICOM file which is imported, processed, displayed and utilized by both our standalone system (MATLAB based) and the actual treatment system. This was to help us determine the exact position of the HDR source and the path it follows. The information gotten from this is used to reconstruct the source, the applicator, and their path, and display it on our GUI. The accuracy of the system can be checked by comparing the coordinates of the reconstructed source to the coordinates of the planned dwell positions of the treatment plan. While the actual treatment machine can easily work with this plan, we are designing our system to work with it as well as will be seen below.

During brachytherapy treatment, the x-ray source is placed at dwell positions for a given dwell time. Dwell positions are distances measured with respect to a reference point. In our experiment, the tip of the test catheter was considered as the reference point as well as the 1st dwell position.

The after-loader delivers the source from one of its output channels to the test catheter via guided tubes. The test catheter is positioned at the isocenter[1]. In radiation physics the isocenter is the point in space through which all the radiation beams intersect and the central beam passes through. The Acuity machine software allows the user to adjust the distance between the isocenter and the detector. Therefore, the catheter had to be placed at the isocenter. Figure 39 represents the schematic for the test plans.

Following the same system of axes, the tip of the catheter is placed at the isocenter. The system of axes is chosen such that the isocenter falls on the z-axis. Once the catheter is located at the isocenter, the source-detector distance can be adjusted with the help of the simulation software of Acuity.

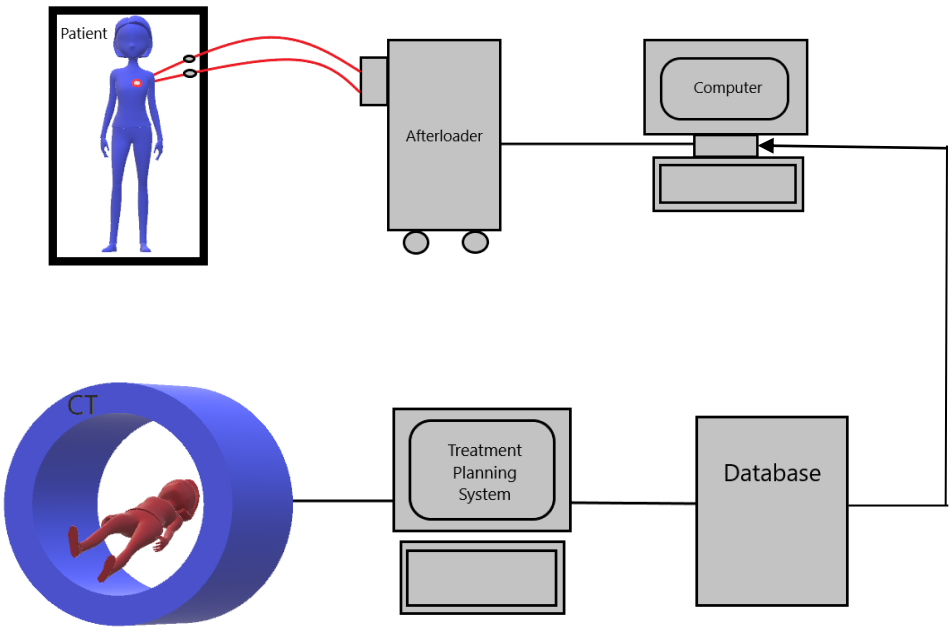

Figure 38: Schematic explaining the test planning and treatment delivery

The catheter arrangement is placed on the operating couch and the flat panel detector is kept parallel to the couch. The catheter is aligned along the x-axis with its tip on the z-axis at the desired height from the detector. By this arrangement, the source will only move along the x-axis with respect to the tip of the catheter, while its position on the y-axis and z-axis remains constant.

The exact length of the guided tube as well as the length of the catheter must be measured and known. In other to send the HDR source to the first planned dwell position. This is done via a measuring wire which measures the distance the source has to travel from the output channel of the after-loader to the tip of the guided tube. The length of the catheter is added to this distance to get the start point that the after-loader must send the HDR source, so that it is delivered at the first planned position. This QA procedure must be followed before every treatment.

The second phase of the brachytherapy treatment plan is setting the dwell time. This is the amount of time for which a source will remain at a given dwell position.

Image acquisition was done via C codes, with the intention to later wrap this code as a MEX file, and repeat the same thing using a GUI. The number of images and the directory to which they were to be saved for easy access, as well as several other properties was specified within the C codes.

3.7 Trials

A test plans was created to mimic an actual clinical scenario. The plan was created on the software that controls the afterloader. This was to help us determine the exact position of the HDR source and the path it follows. Once the exact planned 3-D coordinates of the treatment trials are known, images are acquired using the HDR source and used to reconstruct the source. The accuracy of the system can be checked by comparing the coordinates of the reconstructed source to the coordinates of the planned dwell positions of the treatment plan.

In the previous research, 50cm to 70cm was observed to be a comfortable distance to place the detector from the patient's-HDR-source, in other to get good quality images and retrace the path of the source. That concept was employed in this research as well.

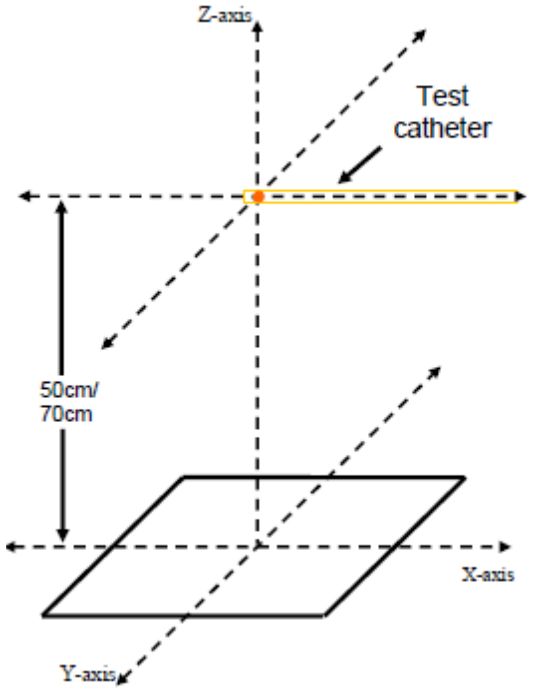

Figure 39: Schematic explaining the positioning of the test catheter and the test plan

3.8 Image Acquisition

Image acquisition was a very critical process since we were using a new detector; the Paxscan X-ray detector. As compared to the previous study on this subject [1], our planned method of image acquisition here is via a C language code, incorporated into a MATLAB GUI. Initially, images were grabbed using the VIVA software provided by the manufacturers of the detector, but this

doesn't give us the flexibility that we need to design our custom program which was used to acquire our images, using the developer resources provided. The Varex detector allows us to acquire images in four distinct modes: fluoroscopy (fluoro) mode, dynamic gain mode, dual gain mode, and radiation (rad) mode.

In fluoro mode, image acquisition is continuous, while in rad mode, images are acquired under software or hardware handshaking control; typically, one image is acquired and saved, though if the number of accumulation frames is set to more than one, then the sum is formed[29]. In dual gain mode each pixel is read at high and low gain. Dynamic gain mode is a special dual gain mode in which each pixel value is read once only at high or low gain; this mode is also referred to as dynamic gain switching (DGS)[29]. In this research we used the fluoroscopy acquisition mode.

The original C code provided by Varex, was written around 2009 or earlier using visual studios. The code has certain dependencies which could potentially stop it from working completely, or even when it does work at-times, it just doesn't give the expected result. Two notable dependencies come from the software setup file that installs the detectors original software (VIVA – Paxscan Virtual CP L07). First is the ebus driver (PaxscanPleoraSupport) which helps establish communication between the host computer and the detector, then the manufacturer driver. The manufacturer driver install option comes after the ebus driver has been installed and isn't stated in the installation manual. One must be careful to ensure that both are installed to avoid strange errors and problems. Another dependency is the Visual C++ redistributable 2010 version; the exact version is shown in Figure 40 below. The installation of this Visual C++ dependency can be done in one of two ways. First is by, downloading the exact version from the Visual studios website, and installing it or second (recommended), by uninstalling all version of Visual C++ redistributable above 2009. By doing this, when the VIVA setup file is run it automatically installs the needed version. Note that there would be an installation error if any version above 2009 is already installed and the installation process might need to be restarted. After installing this dependency you'll need to reinstall the redistributable file for the version of Visual studios that you have installed on your PC. For example, if you have visual studios 2017, then you should also have the 2017 redistributable installed after this.

Finally, the receptor setup file (444S03-0705 folder) that comes from Varex must be copied and pasted in the IMAGERs folder[29], or any other folder where you want the recorded images to be stored, else the entire C program or software won't be able to grab images.

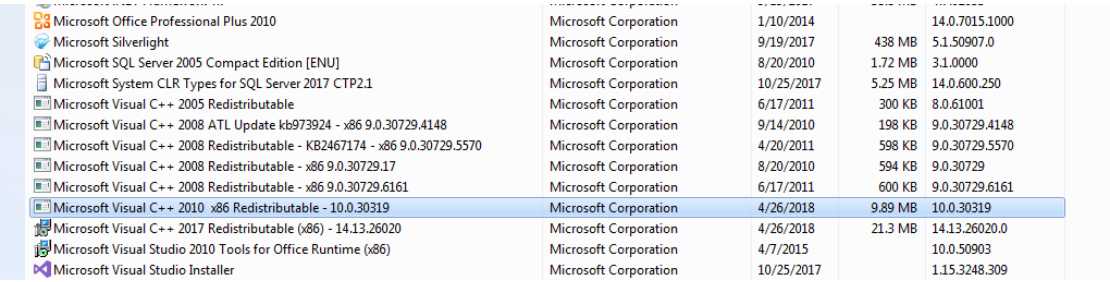

Microsoft Office Professional Plus 2010	Microsoft Corporation	1/10/2014		14.0.7015.1000
Microsoft Silverlight	Microsoft Corporation	9/19/2017	438 MB	5.1.50907.0
Microsoft SQL Server 2005 Compact Edition [ENU]	Microsoft Corporation	8/20/2010	1.72 MB	3.1.0000
Microsoft System CLR Types for SQL Server 2017 CTP2.1	Microsoft Corporation	10/25/2017	5.25 MB	14.0.600.250
Microsoft Visual C++ 2005 Redistributable	Microsoft Corporation	6/17/2011	300 KB	8.0.61001
Microsoft Visual C++ 2008 ATL Update kb973924 - x86 9.0.30729.4148	Microsoft Corporation	9/14/2010	198 KB	9.0.30729.4148
Microsoft Visual C++ 2008 Redistributable - KB2467174 - x86 9.0.30729.5570	Microsoft Corporation	4/20/2011	598 KB	9.0.30729.5570
Microsoft Visual C++ 2008 Redistributable - x86 9.0.30729.17	Microsoft Corporation	8/20/2010	594 KB	9.0.30729
Microsoft Visual C++ 2008 Redistributable - x86 9.0.30729.6161	Microsoft Corporation	6/17/2011	600 KB	9.0.30729.6161
Microsoft Visual C++ 2010 x86 Redistributable - 10.0.30319	Microsoft Corporation	4/26/2018	9.89 MB	10.0.30319
Microsoft Visual C++ 2017 Redistributable (x86) - 14.13.26020	Microsoft Corporation	4/26/2018	21.3 MB	14.13.26020.0
Microsoft Visual Studio 2010 Tools for Office Runtime (x86)	Microsoft Corporation	4/7/2015		10.0.50903
Microsoft Visual Studio Installer	Microsoft Corporation	10/25/2017		1.15.3248.309

Figure 40: Shows a highlight of the exact version of Visual C++ Redistributable 2010 that software and custom code depends on.

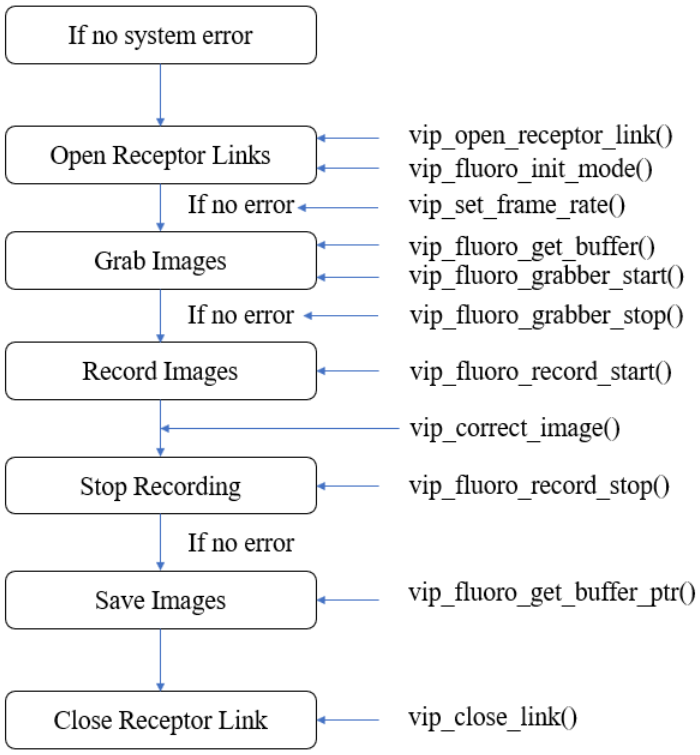

Figure 41: Structure of image capturing program

Figure 41 above, gives a clear and brief description of the operation of the C code used to get the images. Before we delve into much detail about Figure 41, it's important to know that certain standards must be met for the code to operate as desired. First, all calibration and configuration files must reside on the host computer while software runs on it. VirtCplib which is a library that was provided with the sample code provided by Varex, expects all these calibration and

configuration files to be organized into a fixed tree of subdirectories. It is very important to note that the root of this subdirectory tree may be chosen by the user, but the recommended configuration (the VIVA default) is to name the directory IMAGERs (C:IMAGERs), with one or more subdirectories whose names are the serial numbers of the receptor panels that have been installed[29]. This path is saved in the registry and only needs to be set once on any computer.

The VirtCP.dll provided by Varex, reads in calibration files so that it can correct raw images acquired from the X-ray imager panel. The files are read when vip_open_receptor_link() is called: the RecDirPath member of the SOpenReceptorLink structure is expected to be a path name to the calibration tree. The recommended convention is to name this tree C:\IMAGERs\serialnbr. For example if the imager serial number is 1234-56, this path is C:IMAGERs\1234-56[29]. VirtCp.dll is dependent on four other dlls, and at run-time a user links it to them when the receptor link is opened, the include: HcpImgAcq.dll which controls image acquisition and interfaces to I/O devices which may control the x-ray generator; HcpRecCtrl.dll which controls the receptor, stores information parsed from the receptor configuration file and interfaces to frame grabber module; HcpCorrections.dll which performs image corrections and processes calibration data; and HCPCalibration.dll which controls acquisition of calibration data. These four modules in turn generally have other device-specific dependencies[29]. Severally other .dll-extension files are provided with the program, and to avoid any run-time-errors or problems in general, they were also placed in the folder where are had all the codes. One important thing to also look out for when reading through the resources (codes) provided by Varex is that function names are prefixed with vip_(small letters) and constants are prefixed with VIP_ or HCP_ (capitalized for both cases).

Now we're set to describe the program/code structure and working pattern. First, our program includes an error check because there are many challenges that could be experienced practically when the detector is exposed to radiation, or when dealing with. Our expectation is that it works as desired and that when it isn't some sort of notification should be sent to avoid any major problem. After error check is passed, vip_open_receptor_link() proceeds to open receptor link; this must be done before nearly any function is called. While opening receptor link the receptor mode is also set (vip_fluoro_init_mode()), in this case it's set to fluoro mode. After that we set the frame rate, which could be entered as a fixed number or set to '0' which represents continuous image acquisition. Now, vip_fluoro_get_buffer_ptr() points the program to a memory block which receives the image. This memory block must be at least (2 * x-size * y-size) bytes; once the receptor is recognized vip_fluoro_grabber_start() starts grabbing the images an sending them to the allocated block. In our case we get an image size of approximately 7MB (7,798,784Bytes), which is the product of (2*2176*1792).

Vip_fluoro_grabber_start() works in conjunction with the vip_fluoro_get_prms call which provides the range of available indices. There are normally two grab buffers allocated which are accessed directly by the frame grabber. It will normally write to these buffers alternately – 'ping-pong' fashion after a call is made to vip_fluoro-grabber_start(), and continue doing so until

vip_fluoro_grabber_stop() is called[29]. Pleora (driver) provides a buffer class which allocates multiple buffers for a single class object. At this point vip_fluoro_record_start() starts copying image frames from the grab buffers to sequence buffers, beginning with buffer index 0 -until vip_fluoro_record_stop() is called or the requested number of frames have been captured. Corrections are also made simultaneously/are automatically applied in fluoro-mode if necessary by vip_correct_image(). If a specific number of frames is requested, at least that number of buffers must be allocated. If acquisition is free-running then buffers are written in circular fashion, meaning that once the allocated buffers have been filled, the earliest frames acquired will be overwritten. Note that if this happens and the sequence acquisition is stopped arbitrarily, the sequence 'start index' will generally not be zero. The start index may be discovered after the sequence has stopped by calling vip_fluoro_get_prms() referencing SSeqStats.

After vip_fluoro_record_stop() function is called and no more frames is been copied to the sequence buffers, and error check is done, if this passes, vip_fluoro_get_buffer_ptr() function repoints to the location (directory) where our images will be saved. When this process complete, vip_close_link() function closes the link. The close function is very important and should only be done when the acquisition session is finished. This function frees some of the resources and memory associated with the receptor. Memory allocated for sequence buffers is by default not deallocated until VirtCp is detached. This behavior can be modified by following the instructions in the user manual[29].

Prior to running the test plan, we acquired images using our native codes without the HDR source. This raw image as shown in figure 42 below is used for morphological image processing.

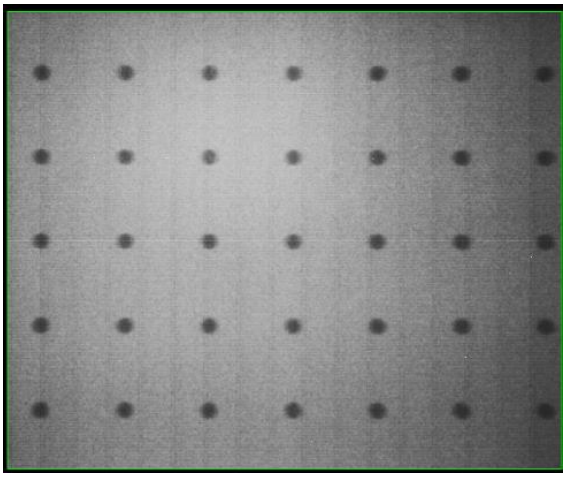

Figure 42: Raw greyscale image from detector

They are subtracted from the images acquired with the HDR source. At this point the result of such subtraction consider any exposure or noise produced by the leakage of x-ray from the source. A series of images were further taken by the afterloader at distinct planned dwell positions. The images produced were a projection of the markers on a setup mounted on the flat panel detector and placed between the HDR source sent by the afterloader and the flat panel detector as shown in figure 43 and 44 below.

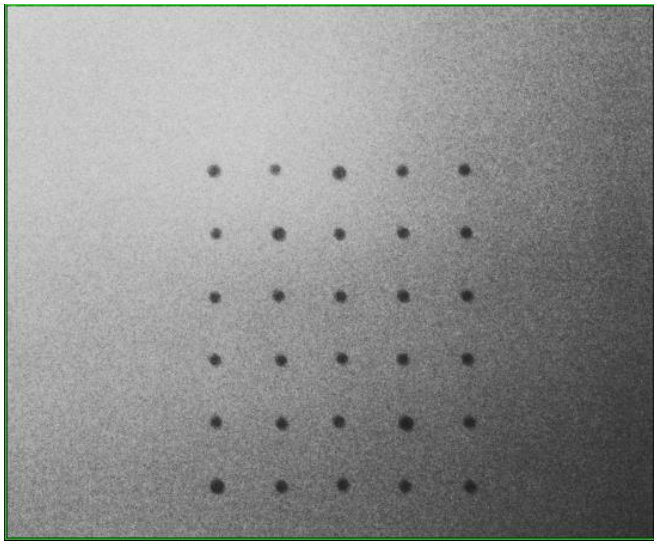

Figure 43: Filtered raw image

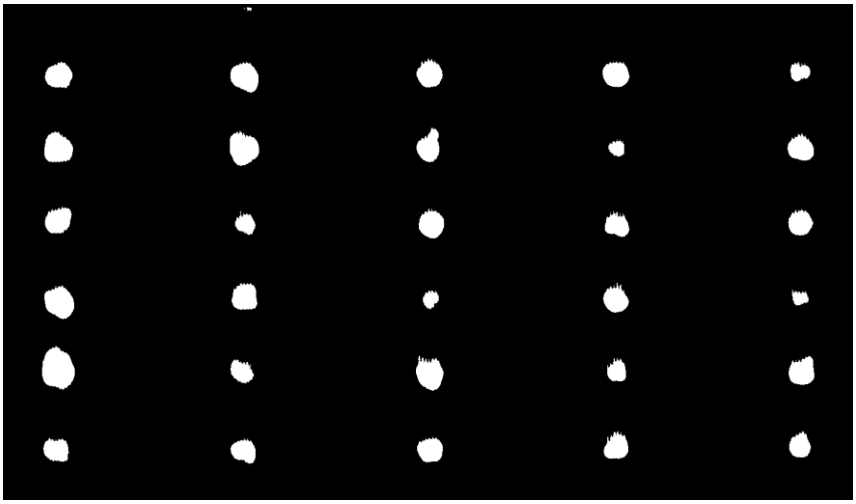

Figure 44: Result of Subtraction of filtered image

Dwell time was set such that we that we could take good sets of images, but normally images acquisition took less than 10seconds when all parameters for image acquisition were set and in place. The images were acquired and saved via a custom MATLAB GUI which calls in a C-function to communicate with the detector and acquire the images. The acquired images are saved in ".raw" format, read into MATLAB processed and saved in DICOM form. The images acquired here show significant improvement from that taken using the previous detector, but we still did an averaging over five images to get a better image and reduce noise significantly. The concept behind averaging is that random fluctuations of the noise above and below the projection of markers will gradually cancel each other out, thus improving the signal to noise ratio.

Noise at the edges where cropped out by pixel adjustment, using the code structure below:

```
I=X(26:743,26:999);
```

Where X is the original image after image averaging and the cropped image is stored a new variable I. One noticeable improvement of the new detector is its resolution of 2176 by 1792, and better sensitivity of its receptors.

3.8.1 Morphological Image Processing

Now that we have our noise-reduced-images saved in DICOM format, they are now ready for processing in MATLAB. The images are processed at this point to fathom, the 3-dimensional

coordinates of the projection of the markers. The centroids of the projection of the marker on the acquired images are used as surrogates for the 3-dimensional coordinates[1].

At this point morphological image processing is performed on our image to isolate the shape and size of the markers and obtain the coordinates of the centroid. 'imbothat' command from MATLAB image processing toolbox was used to perform bottom-hat filtering on our grayscale image. The bottom-hat filter requires a structuring element which would define the shape of the markers[1]. Since the markers are circular structures we define a structuring element of type 'disk' using the 'strel' function. The filtered image is then stored as a new variable. Below is an example of the using of both functions.

```
Se = strel('disk',25);

I1 = imbothat(I,se);
```

The codes above create a flat disk-shaped structuring element 'se' with a radius of 25 pixels. The bottom-hat function is performed on the cropped image 'I' using 'se' and stores it in I1. Apart from the bottom-hat filter, wiener2 and medfilt2 filters were also used. Wiener2 is a 2-D pixelwise adaptive Wiener filtering method which acts as a lowpass filter to improve a degraded grayscale image by removing the noise; it works based on statistics estimated from a local neighborhood of each pixel [1]. Medfilt2 on the other hand is a two-dimensional median filtering technique which is used to reduce tiny pixels of noise. The code for both filters are given and explained below.

```
[I2, noise] = wiener2(I1,[15 15]);

I3 = medfilt2(I2,[8 8]);
```

In the first line, a 15 by 15pixel size neighborhood was used to estimate the local image mean and standard deviation to perform the wiener2 filtration function on the image labelled I1, and the filtered image is stored in I2. In the case of medfilt2, an 8 by 8pixel size neighborhood was used around each pixel in I2 to perform median filtration. The filtered images were then stored in I3.

After these we are set to isolate the markers as a next step. The grayscale image is converted into a binary image such that only the markers take the value 1 while the rest of the image is 0. This is done by applying a threshold to the image, as shown below.

```
I4 = I3>mean2(I3) + 2.5*std2(I3);
```

From the code above, the mean value is added to 2.5times the standard deviation value and used as a threshold which is applied to image I3 and the resulting binary image was stored as a

variable I4. From I4, the markers can be isolated, labeled and the centroids for each marker can be calculated using the code described below.

```
[I5,NUM]=bwlabeln(I4);

STATS=regionprops(I5,'Centroid','Area');
```

The 'bwlabeln' jfunction labels the markers in the image I4 and stores the result in variable I5. "regionprops" function measures the centroid and area of the labeled markers in the image I5 and stores it in the array STATS. The x-y pixel coordinates of the centroids can be accessed using the Comma-Separated List Syntax as explained below,

```
STATS.Centroid
```

The centroid acts as substitute for the coordinate of the markers and is represented by the pixel number. To obtain the coordinates with respect to the system of axis that we chose, the x and y coordinates of the pixel number of the centroid must be subtracted from the center of the detector. The coordinates are converted into centimeters by multiplying the pixel number with the pixel size or the resolution of the flat panel detector.

As compared to the previous work on this research where the detector, was set at half resolution, we used the full resolution in this case with a pixel size of 0.0388cm. Converting pixel numbers to centimeters simplified calculations for the reconstruction of the source. The same procedure was carried out for the calibration image and the 3-dimensional coordinates of the markers were also converted into centimeters. Figure 45 depicts a segmented and labeled image which was acquired for the first dwell position of the second test plan.

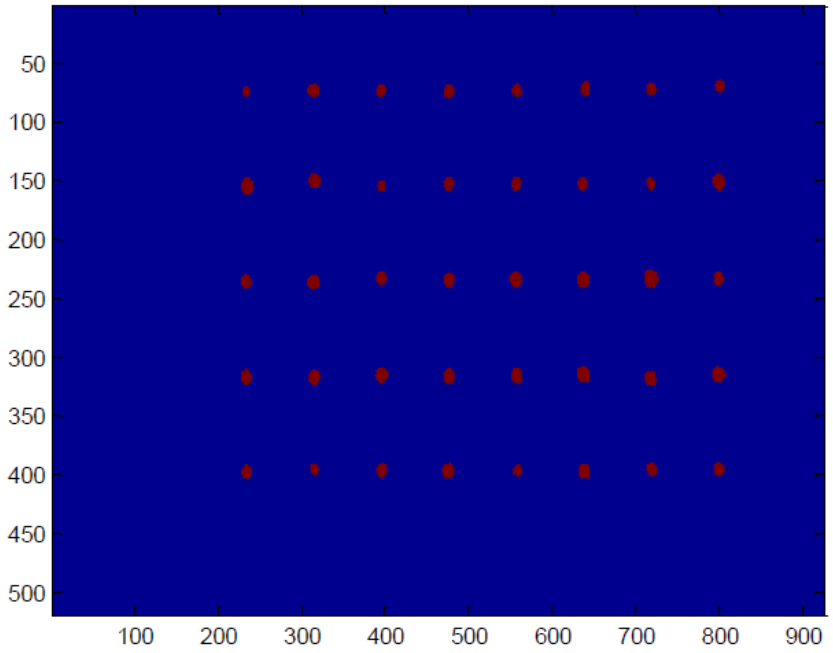

Figure 45: Binary image obtained after morphologically processing and segmenting the grayscale image.

3.8.2 Reconstruction of the source

Since the goal of this research is strongly related to locating the source position, much attention was given to this section. After analyzing the images for all dwell positions for all the test plans it was observed that the coordinates of the projections of the markers were unique for each dwell position. This demonstrates that the coordinates of the projection of the markers are correlated to the position of the source. The calibration method gives the exact 3-D coordinates of the markers. The exact 3-dimensional coordinates of the projection of the markers are further obtained by processing the images acquired using the HDR source. Using these 3-D marker coordinates and projections, the positions of the source is formed by pairing each marker with its projection and calculating the shortest distance. This we did by providing a label to each blob on the marker image and the projection image and with the help of the label number the marker is paired with its respective projection.

After labelling the segmented image, the markers get labeled in any random order. Thus the labelled markers needed to be rearranged such that we have the same order for the markers

on the calibration image and the projection of the marker on the image acquired via the HDR source. This makes the pairing of markers with its respective projection much easier. “sort” command in MATLAB was used to perform this function. It sorted the coordinates of projections and stored them in a variable called ‘img’ while the sorted coordinates of the markers are stored in a variable called ‘cal’.

Lines in 3-D are defined with the help of the 3-D coordinates of the marker and its respective projections. Two lines defined by two marker-projection-pair are used at one time. The intersection of both lines defined the source position. The intersection of the two lines in 3-D is very unlikely practically, so a method was devised were the shortest line segment which connects the two lines in 3-D was used for further computation. This line segment is considered the intersection of both lines.

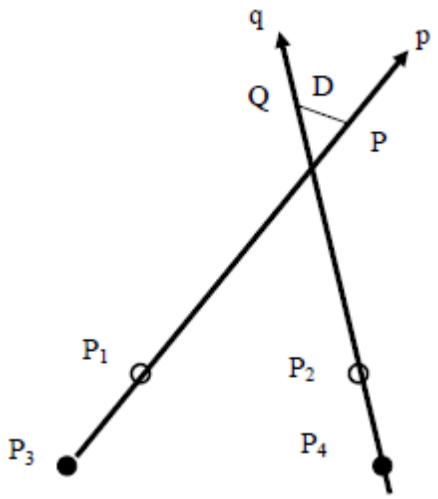

Figure 46: Intersection of two lines in 3D[1].

From the figure 46, line p is defined by the marker P_1 and its projection P_3 and represented by the equation 1; line q is defined by the marker P_2 and its projection P_4 and is represented by the equation 2

$$P = P_1 + mu_p * (P_3-P_1)----------(1)$$

$$Q = P_2 + mu_q * (P_4-P_2)----------(2)$$

P and Q represent the points on the lines p and q which give the shortest distance between the two lines. The values of mu_p and mu_q range from negative infinity to positive infinity.

The shortest line segment between the two lines should be perpendicular to the two lines. Thus, two equations for the dot product are represented as

$$(P-Q)\ dot(P_3-P_1)=0$$

$$(P-Q)dot(P_4-P_2)=0$$

Expanding the above equations using 1 and 2 we get,

$$(P_1-P_2+mu_p*(P_3-P_1)-mu_q*(P_4-P_2))dot(P_3-P_1)=0$$

$$(P_1-P_2+mu_p*(P_3-P_1)-mu_q*(P_4-P_2))dot(P_4-P_2)=0$$

Both equations above represents two equations with two unknowns mu_p and mu_q, thus solving the above two equations simultaneously gives the values of mu_p and mu_q. The coordinates of P and Q is derived by substituting these values in equations 1 and 2. The mean of P and Q is used as the position of the source.

The procedure above is repeated for all the possible combination of marker projection pairs. Thus, N markers would produce N*(N-1)/2 combinations of marker-projection pairs, each pair given a shortest distance D and a P and a Q. The mean over all the P's and Q's will give the most accurate position of the source.

The above processes, were all implemented via MATLAB: the reading of the five DICOM images, the calibration image and the blank image; averaging and subtraction of images for noise cancellation, system calibration, segmenting and labeling of all the HDR images, calculating the coordinates for the calibration of HDR images, sorting out the labelled images, pairing the markers with their respective projection and finally calculating the shortest distance and the coordinates for the points of intersection. This helped us locate the position of the source in 3D and implement the entire process in MATLAB.

3.9 GUI Design

All the monitoring operations of our standalone system will be performed by the MATLAB GUI in Figure 48 below. The entire testing processes described above, from image acquisition through source reconstruction, will be controlled from the GUI. The GUI interface is programmed such that on clicking the start tracking button, all the functions associated with the tracking process begins to run, and the desired output are displayed in the axis. These processes

will include the image processing procedures listed below, arranging as sequential function within our code:

- Image Enhancement – Noise removal, deblurring, filtering
- Image Segmentation
- Image Analysis
- Morphological Operations

The codes for these image processing procedures were mostly gotten from previous research on this topic. While the code that acquires the image, and the MEX file, and GUI and a few other extra codes are a product of this research.

It is assumed that by using all the results from all the codes run by our standalone system, the changes in the source position could be tracked as shown in the image below.

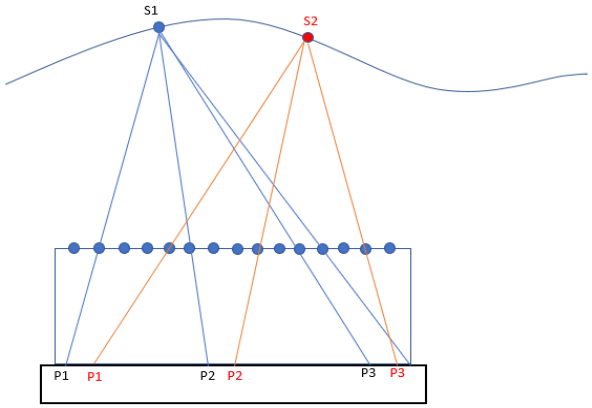

Figure 47: Effect of change in source position

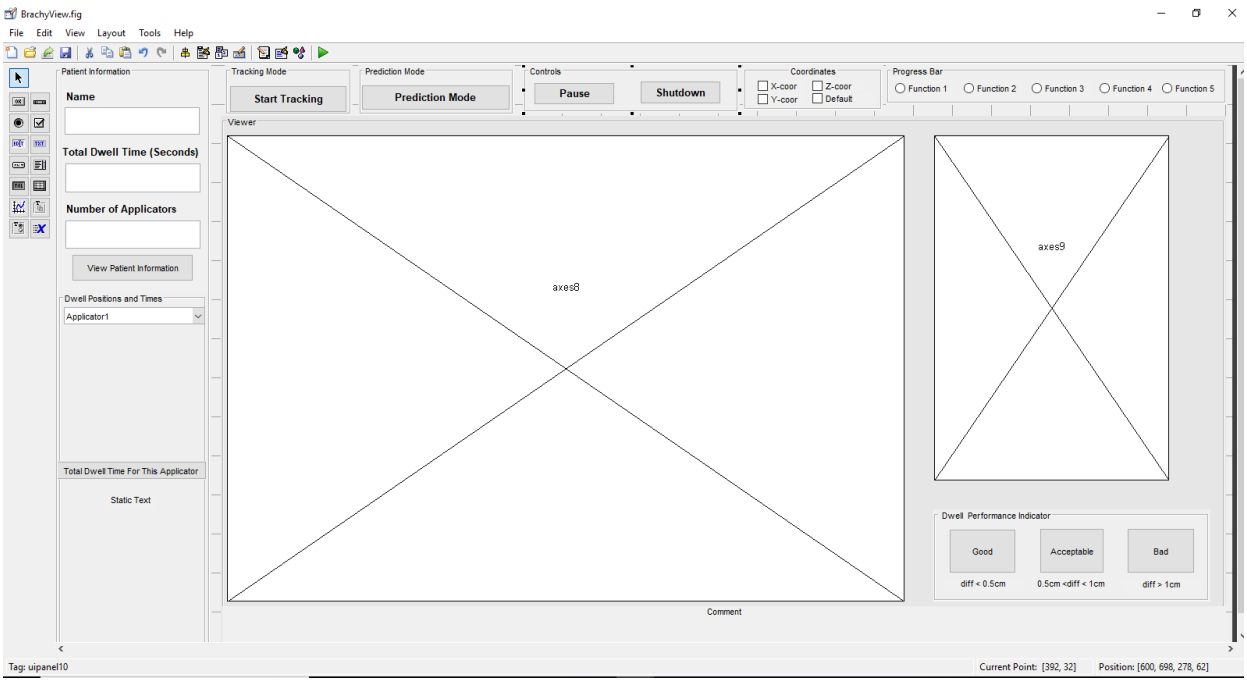

Figure 48: MATLAB GUI

3.9.1 Tracking Versus Prediction Mode

Figure 49 below gives a glimpse of what tracking mode signifies. In this mode the movement of the source along the catheter is monitored on the GUI in real-time, while treatment supposedly takes place. By default, our system runs in this mode when the “Start Tracking” button in Figure 49 is clicked. In this mode the source path is also plotted, and several other information can be found on the GUI.

Prediction mode makes a little change to the GUI. This mode is activated by clicking on the “Prediction Mode” button on the GUI. In this mode the system check if the source is in a dwell given position for a given time and if it meets the quality assurance standard predefined by us. If the standard is not met, indicators (green, red, yellow indicators) will begin to blink on the GUI to inform us of the degree of violation of our set standard. This way we can know if we need to shut-down treatment and what step to take. In prediction mode, the system also keeps record of passes and fails for the dwell positions and their corresponding dwell times.

App.2	App.3	App.4	App.5	App.6	App.7	App.8	App.9	App 11	App 12	App 13	App 14
0	0	0	0	0	0	0	0	0	0	0	0
0.1	0.2	3.0	1	3.2	4.4	0.1	4.2	1.5	3.0	1	1.2
0.1	0.2	3.0	1	3.2		0.1	4.2	1.5	3.0	1	1.2
5.0	1.9	4.5	1.7	3.2		4.0	5.6	4.1	4.1	1.7	1.3
5.0	1.9	4.5	1.7	3.2		4.0	5.6	4.1	4.1	1.7	1.3
5.0	4.9	4.6	3.3	6.0		4.7	6.6	4.6	4.2	2.1	1.8
5.0	4.9	4.6	3.3	6.0		5.0	6.6	4.6	4.2	2.1	1.8
5.4	5.2	6.0	4.7	6.8		5.0	6.7	7.0	10.6	2.5	2.5
5.4	5.2	6.0	4.7	6.8		6.1	6.7	7.0	10.6	2.5	2.5
8.7	7.3	8.0	4.7	9.3		6.1	7.6	10.1	10.7	3.1	2.8
	7.3	8.0	4.7	9.3		8.5	7.6		10.7	3.1	2.8
	7.6	8.5	6.8	10.2		8.5	7.8		11.0	3.3	2.9
	7.6	8.5	6.8	10.2		8.6	7.8		11.0	3.3	2.9
	8.1	8.5	8.7	13.9		8.6	8.4		13.3	3.6	3.0
	8.1	8.5	8.7	13.9		9.2	8.4		13.3	3.6	
	8.1	9.9	8.8	13.9			8.5		15.1	5.2	
	8.1	9.9	8.8	13.9			8.5		15.1	5.2	
	9.6	10.2	9.9	16.2			8.8		15.8	5.7	
	9.6	10.2	9.9				8.8		15.8	5.7	
	9.9	10.8	10.6				8.9		17.6	6.1	
	9.9	10.8	10.6				8.9		17.6	6.1	
	10.2	11.5	15.5				9.2		17.8	6.4	
	10.2	11.5	15.5				9.2		17.8		
	11.9	12.5	16.0				10.3		18.8		
	11.9	12.5	16.0				10.3		18.8		
	12.7	13.5	17.1				11.4		20.1		
	12.7	13.5									
	15.2	16.1									
		16.1									
		16.1									

Table 1: Cumulative-time-weights for the all dwell positions in each catheter arranged sequentially as a factor of time (Nth second at Nth Position)

From Table 1, applicator 2 has 10 dwell positions, applicator 3 has 28 dwell positions, applicator 4 has 30 dwell positions, applicator 5 has 26 dwell positions, applicator 6 has 18 dwell positions, applicator 7 has 2 dwell positions, applicator 8 has 16 dwell positions, applicator 9 has 26 dwell positions, applicator 11 has 10 dwell positions, applicator 12 has 26 dwell positions, applicator 13 has 22 dwell positions, and applicator 14 has 14 dwell positions.

In other to create a MATLAB function that simulates the source movement, we applied differential equation to the cumulative-time-weights for the various dwell positions for each catheter. The code below shows the logic applied.

DwellT_Item1=diff(CTimep(1:10));

This equation displayed the differences in time for all the Nth-cumulative-time-weights in Table 1 above, belonging to each catheter. By applying this equation to App.2 (Table 1) for example, we got: 0.1, 0, 4.9, 0, 0, 0.4, 0, 3.3. Another MATLAB algorithm as seen in the equation below, was then applied to remove the zeros, which leaves us with 0.1, 4.9, 0.4 and 3.3.

DwellT_Item12(DwellT_Item12==0)=[];

Adding all this together we get 8.7 which is the last cumulative-time-weight for the source in App.2. These time changes are then used to create Table 2, and the animated simulation of the source movement.

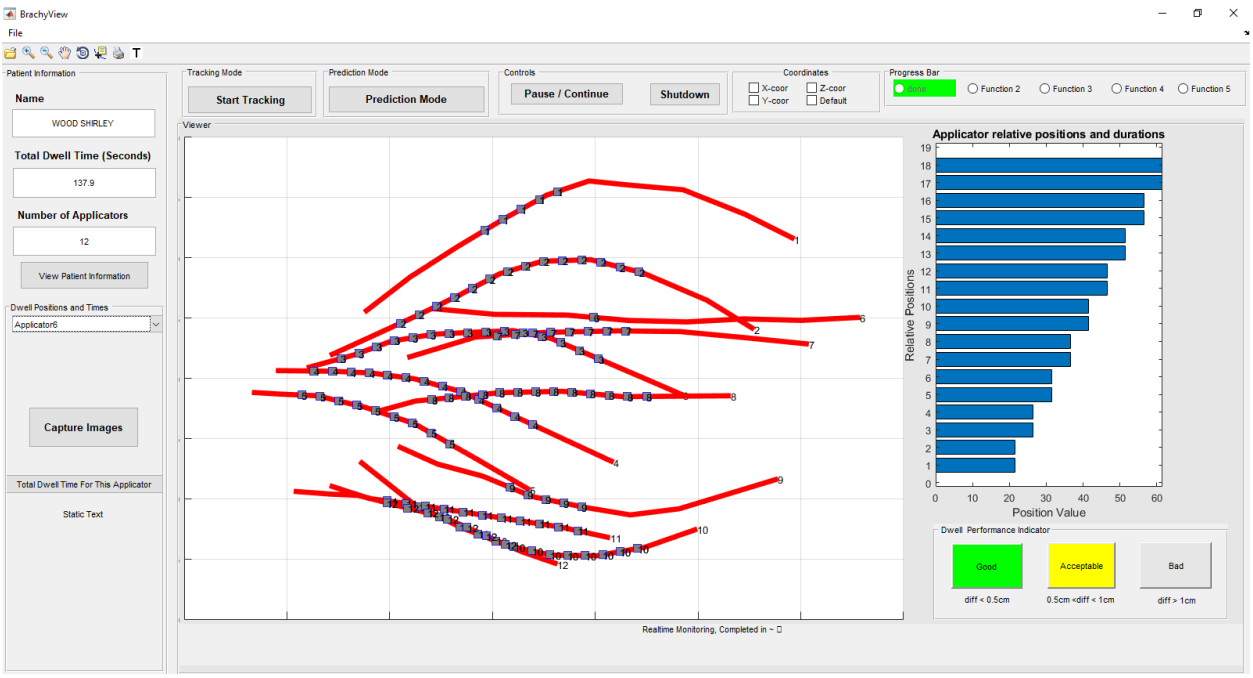

Figure 49: Realtime Simulation in GUI

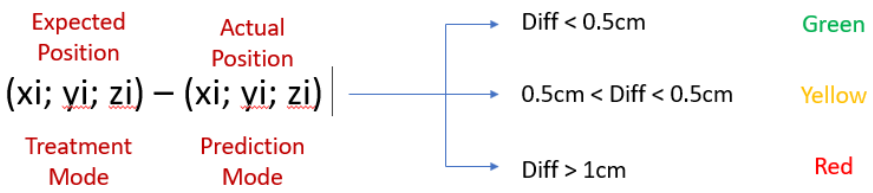

Figure 50: Logic behind prediction mode color indicator in GUI

CHAPTER 4 RESULTS

To test our design a simulation which portrays the animated movement of the source along several dwell positions was created. This simulation runs without communicating with the detector. The assumption here is that the C-program in the form of MEX file gives absolutely no problem and runs perfectly.

With a total of 113 dwell positions, along 12 distinct channels, the expected total dwell time is 137.9seconds while it took an average actual time of 145seconds for our system to completely run, as estimated by the tic/toc function in MATLAB. This is about 7.1second behind the actual treatment time. In Table 3 though, we got a total average of 151.83seconds, which is roughly 14seconds shy of the expected value. This could be attributed to human error, because the actual-times used to calculate the averages in Table 3 were done using manually using the timer on a phone which definitely influenced its accuracy.

App.2	App.3	App.4	App.5	App.6	App.7	App.8	App.9	App 11	App 12	App 13	App 14
0.1	0.2	3.0	1.0	3.2	4.4	0.1	4.2	1.5	3.0	1.0	1.2
4.9	1.7	1.5	0.7	2.8		3.9	1.4	2.6	1.1	0.7	0.1
0.4	3.0	0.1	1.6	0.8		0.7	1.0	0.5	0.1	0.4	0.5
3.3	0.3	1.4	1.4	2.5		0.3	0.1	2.4	6.4	0.4	0.7
	2.1	2.0	2.1	0.9		1.1	0.9	3.1	0.1	0.6	0.3
	0.3	0.5	1.9	3.7		2.4	0.2		0.3	0.2	0.1
	2.1	1.4	0.1	2.3		0.1	0.6		2.3	0.3	0.1
	0.3	0.3	1.1			0.6	0.1		1.8	1.6	
	0.5	0.6	0.7				0.3		0.7	0.5	
	1.5	0.7	4.9				0.1		1.8	0.4	
	0.3	1.0	0.5				0.3		0.2	0.3	
	0.3	1.0	1.1				1.1		1.0		
	1.7	2.6					1.1		1.3		
	0.8										
	2.5										

Table 2: Shows sequential time changes after applying differential function to Table 1, and taking of the zeros that represents no change

For all the time changes in each column above which represents a movement from one position to another, a radiation of strength: 37552.28 cGy cm^2/h is applied. This is intended to meet the prescription of 3400cGy-in-10-fractions, which is the prescription we created for our sample patient.

Success in Table 3 below, is defined as those points in time when the differences in delay is less than 1.5seconds.

	Expected Cumulative Dwell time (Seconds)	Actual Cumulative Dwelltimes (Seconds)	Averaged Actual Cumulative Dwelltimes (Seconds)	Difference (Seconds)	Failure	Success
Applicator 2	8.7	15.52 14.12 14.18	14.6	5.9	1	0
Applicator 3	15.2	18.27 18.93 18.78	18.66	3.46	1	0
Applicator 4	16.1	14.74 14.60 14.61	14.65	1.45	0	1
Applicator 5	17.1	19.45 19.48 19.65	19.53	2.43	1	0
Applicator 6	16.2	15.86 15.93 15.77	15.85	0.35	0	1
Applicator 7	4.4	6.16 6.52 6.08	6.25	1.85	1	0
Applicator 8	9.2	9.73 7.12 10.13	9	0.2	0	1
Applicator 9	11.4	12.71 8.59 12.45	11.25	0.15	0	1
Applicator 11	10.1	10.36 10.53 10.53	10.47	0.37	0	1
Applicator 12	20.1	21.07 20.82 20.88	20.92	0.82	0	1
Applicator 13	6.4	7.24 7.67 7.09	7.33	0.93	0	1
Applicator 14	3.0	3.30 3.12 3.54	3.32	0.32	0	1
Over All	137.9		151.83		4	8

Table 3: Shows the total number of failures and successful treatment delivery in each catheter

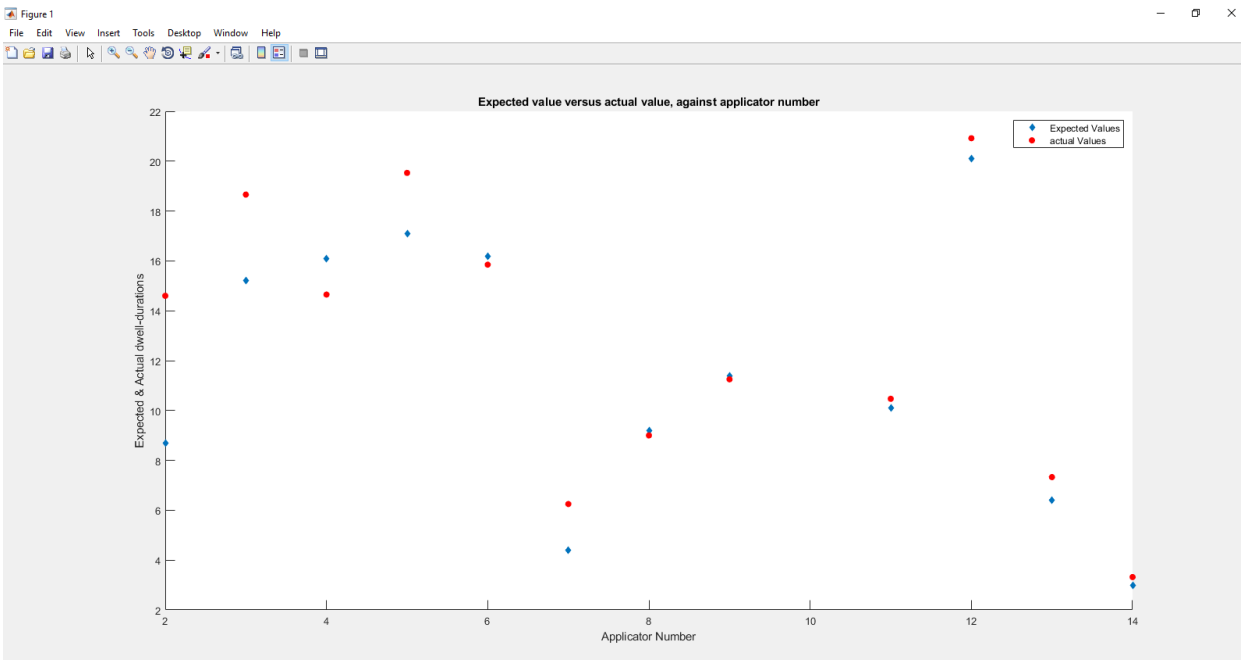

Figure 51: Expected cumulative dwell-times versus actual cumulative dwell-times

From Figure 51, the most deviation of actual dwell-time from the expected dwell-time was in applicator 2. It could be observed when starting the program that there was always a longer time delay at this point, probably because the program had to load the patient's DICOM information from the plan and structure file before displaying any result. Using the 1.50second difference limit as a measure of successes or failure, we could state that there is approximately a 33% chance of failure (4 of 12) and 67% chance of success (8 of 12).

CHAPTER 5 DISCUSSION AND FUTURE DEVELOPMENT

Currently, this system is very sensitive, and numerous errors can occur when working with it, which might require us to restart the monitoring system, and which could result in very bad consequence in the real world. One problem encountered when working with the detector, was that during image acquisition, when the radiation source exited the afterloader the system developed errors and we had to restart the acquisition process. This could possibly be due to communication errors caused by the radiation signals interfering with the signal running in the ethernet cable that connects the computer to the detector. But whatever it was, it seemed to normalize after a while. This didn't always happen as well.

Based on information in the detector user manual, sometimes there are rare cases where firewalls are problematic, in such cases we are provided with the device's media access control address (MAC address) in the HcpConfig.ini file, which comes with the other installation programs.

I also recommend that Visual Studios should be installed on any computer running this program, because some dependencies which it works with might be only accessible from the software, such as Visual C++ VirtCp.dll.

All in all, our system seems to be progressing in the right direction, with many signs of good discoveries that could be made soon. As a final recommendation, I believe this project is possible and it will be more efficient if the final system (after the full system is built) is redesigned in C or C++, because they both perform a lot better when dealing with complex codes like the one used in this project, and image processing of images of size 7MB.

So far, I have been able to find only a single similar work on this topic [17,22], titled BrachyView. In this research, the HDR BrachyView probe is an in-body pinhole imaging system designed for real-time source localization during prostate HDR brachytherapy procedures. In this project they used an arrangement of Source, BrachyView probe collimator (fabricated with cylindrical Tungsten-alloy shell) and pixelated silicon detector material. The collimator has an outer diameter of 24mm, with 7-double-cone-pinholes uniformly distributed across its length with a center-to-center spacing of 6.5mm. The tungsten material used for the collimator was chosen due to its high mass attenuation factor, due to high energy of photons emitted by the Ir-192 HDR source.

The detector is a pixelated silicon detector Timepix, which is a variant of Medipix2 detector. Each pixel in this detector has its own preamplifier, discriminator and counter. The discriminators are used to suppress noise and select the energy range of interest. Each counter can be configured to work in one of three modes: counting the number of detected articles, measurement of particle energy, or measurement of time interaction. A complete imaging system can be assembled from an array of four Timepix detectors and their associated microprocessor-controlled USB-readout system(Fitpix). The Timepix/Fitpix system allows a frame rate of up to 400 images per second to be obtained with very low electronic noise.

The source position is determined using a simple 3-dimensional triangulation method that makes use of the centers of mass of the projected images.

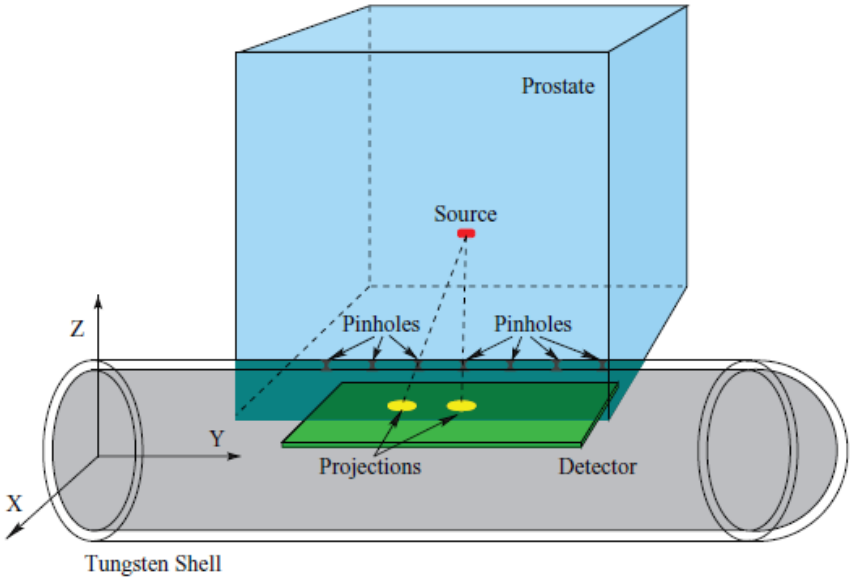

Figure 52: System arrangement [18].

In this experiment, they used the concept that since back-projected lines do not always precisely intersect, the best estimate of the source position is the point with the minimum distance to all the back-projected lines. No source marching is required as well since only a single source is utilized for HDR brachytherapy.

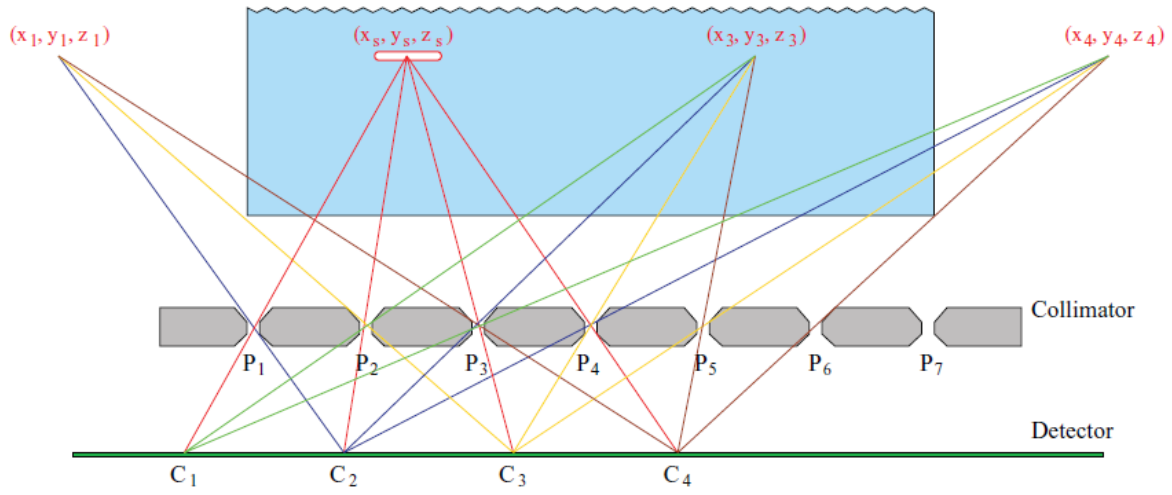

Figure 53: Collimator detector operation [18].

Compared to our work, the above work is abit more invasive. while the system in this research is passive, and in my opinion will be less precise because of the poor image averaging technique employed. Also the detector can be placed no more than 1.5mm above the above the center of the probe cavity to maximize the field of view .

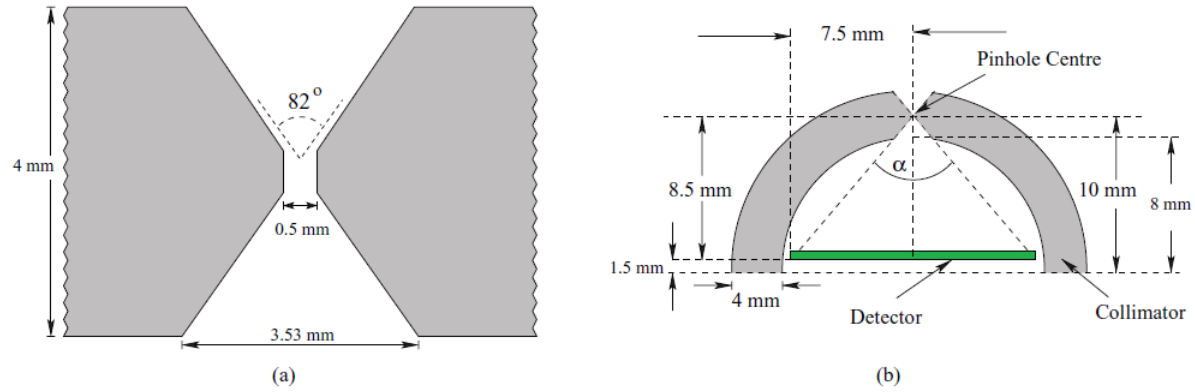

Figure 54: Collimator structure [18].

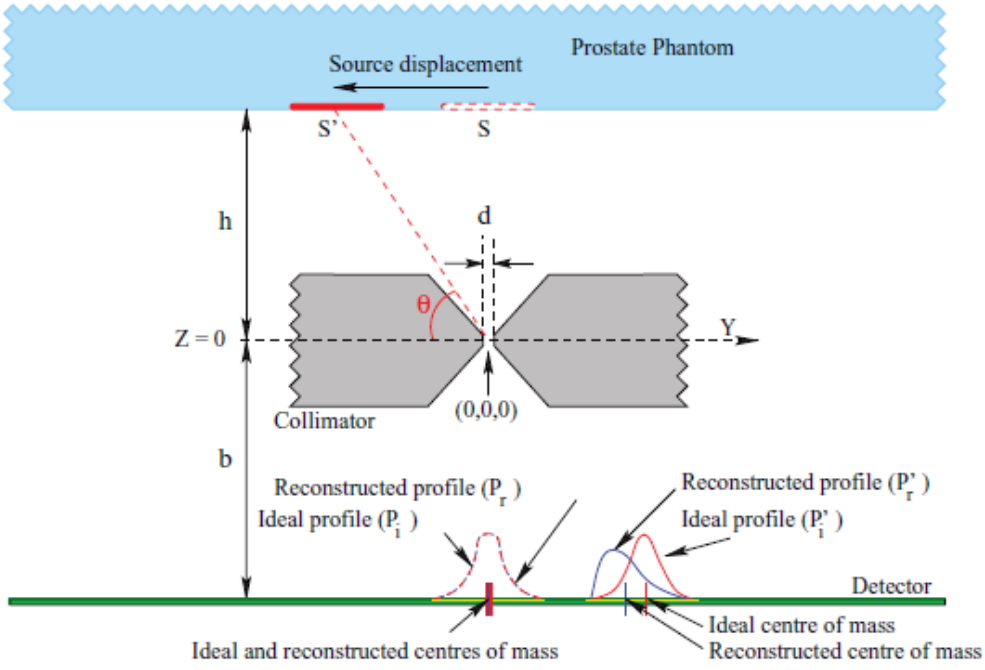

Figure 55: Collimator structure [18].

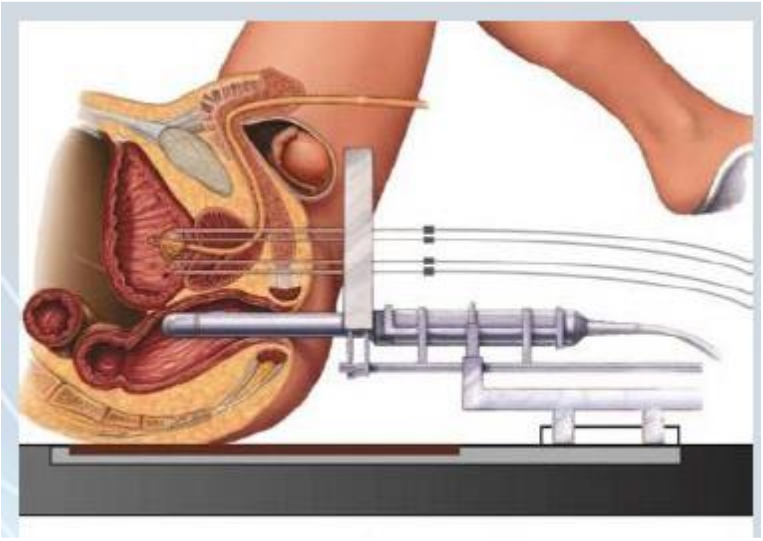

Figure 56: Treatment System Arrangement [13].

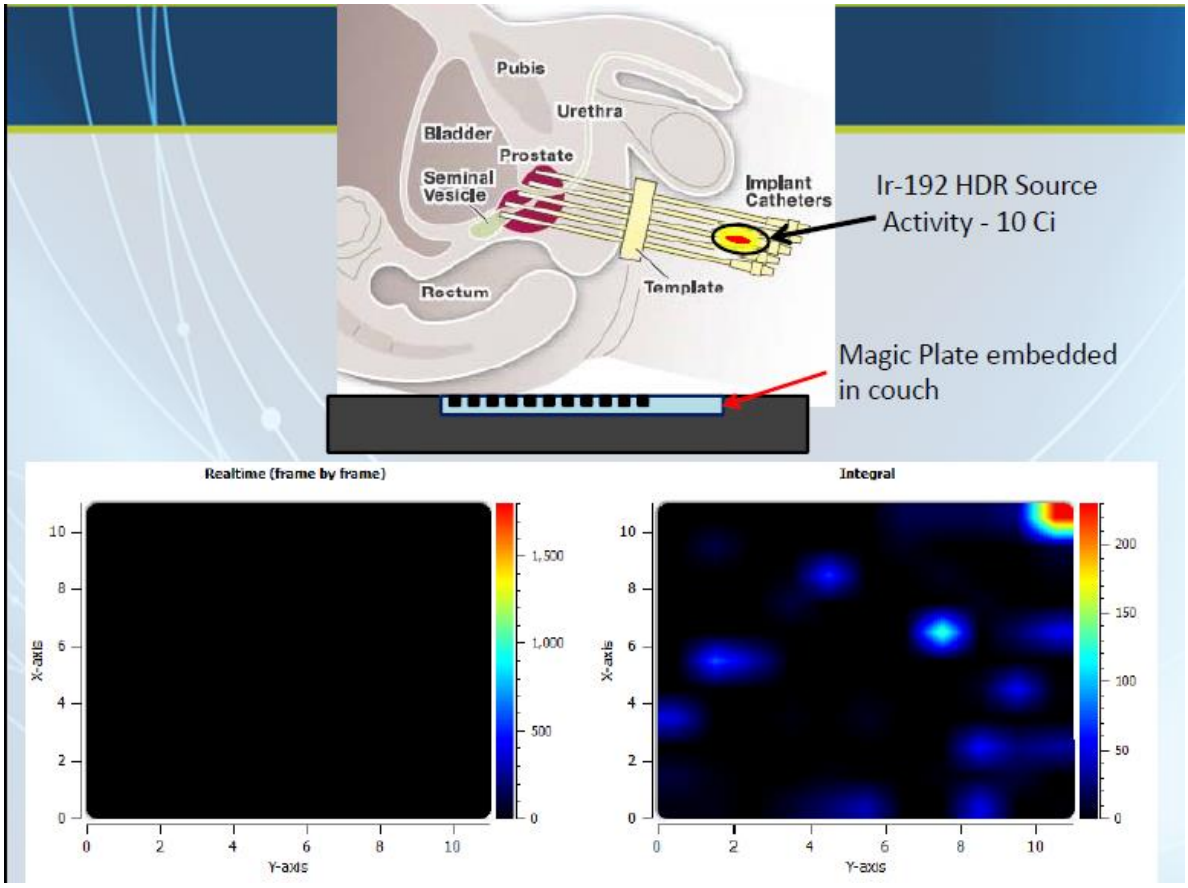

Figure 57: System Arrangement [13].

The models used in their research was designed and simulated in GEANT4 simulation application via MONTE CARLO simulation method, to validate the design.

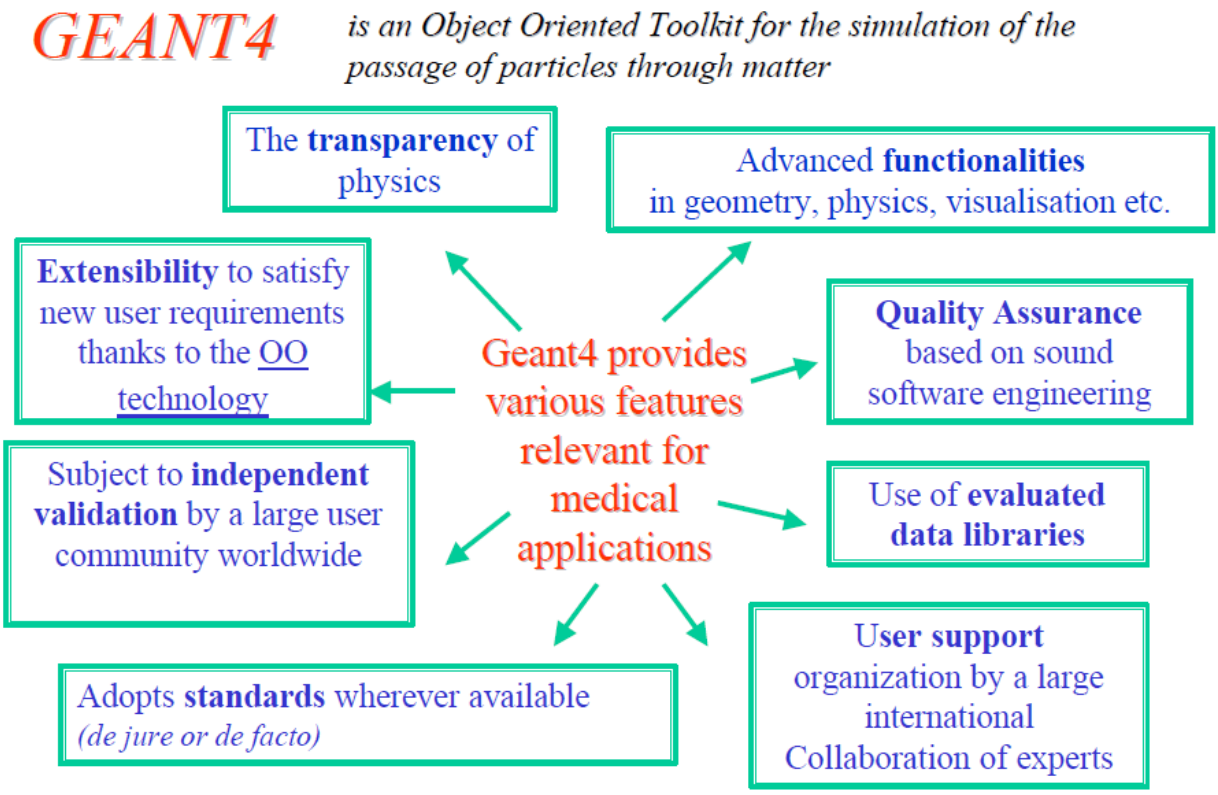

Figure 58: GEANT Simulator Structure [18]

Results from their simulation show that errors in estimating the center of mass of the projection in the detector plane did not exceed 1mm in worst case, and the positioning error decreases as source is placed further away from the collimator.

In summary, running the image processing procedures above, obtaining continuous images using an efficient C code, and integrating all the codes in MATLAB is the main goal of this research. Proper operation, precision-measurement, as well as the addition of any extra intelligence to this system will be a future development.

Reference List

1. Aditya Bondal, Dr Dori Todor, Prof. Fei; “real time 3D tracking of the hogh dose rate radiation source using a flat panel detector.
2. American Cancer Society. *https://www.cancer.org/cancer/cancer-basics/history-of-cancer/cancer-treatment-radiation.html*
3. AmericanBrachytherapySociety.https://www.americanbrachytherapy.org/aboutbrachytherapy/history.cfm
4. Encyclopedia Britannica, Inc. *Breast Cancer*. 2018.
5. Muhammed Murtaza, Sarah Dawson, Dana Tsui, Davina Gale, Tim Forshew, Anna Piskorz, Christine Parkinson, Suet .F Chen, Zoya Kingsbury, Alvin Wong, Francesco Marass, Sean Humphray, James Hadfield, David Bentley, Tan M. Chin, James Brenton, Carlos Caldas and Nitzan Rosenfeld. *Non-Invasive Analysis of Acquired Resistance to Cancer Therapy by Sequencing of Plasma DNA*. May 2, 2013.
6. Wahiba Ben Abdessalem Karaa and Nilanjan Dey. *Biomedical Image Analysis and Mining Techniques For Improved Health Outcomes*. Book 2016.
7. Isabelle Kindts, Annouschka Laenen, Stephanie Peeters, Hilde Janssen, Tom Depuydt, Patrick Neven, Erik V. Limbergen, Caroline Weltens. *Evaluation Of a Breast Cancer Nomogram To Predict Ipsilateral Breast Relapse After Breast-Conserving Therapy*. January 19, 2016.
8. Christine E. Hill-Kayser, David Chacko, Wei-Ting Hwang, Neha Vapiwala, and Lawrence J.Solin. *Long-term Clinical And Cosmetic Outcomes After Breast Conservation Treatment For Women With Early-Stage Breast Carcinoma According To The Type Of Breast Boost*. December 14, 2009.
9. Liv Veldeman, Kimberly Schiettecatte, Charlotte De Sutter, Christel Monten, Annick V. Greveling, Patrick Berkovic, Thomas Mulliez, and Wilfried D. Neve. *The 2-year Cosmetic Outcome of a Randomized Trial Comparing Prone and Supine Whole-Breast Irradiation in Large-Breasted Women*. March 2, 2016.
10. Christopher F Njeh, Mark W Saunders, Christian M Langton. *Accelerated Partial Breast Irradiation (APBI): A Review of Available Techniques*. 2010
11. Cancer Treatment Center of America. *https://www.cancercenter.com/breast-cancer/apbi/* . 2018
12. Tibor Major, Prof. Csaba Polgar. *Treatment Planning For Multicatheter Interstitial Brachytherapy of Breast Cancer – From Paris System To Anatomy-Based Inverse Planning*. February 28, 2017.
13. Jennifer l. Harper, John M. Watkins, A. Jason Zauls, Amy E. Wahlquist, Elizabeth G. Mayer, Megan K. Baker, David J. Cole, Anthony E. Dragun, Joseph M. Jenrette. *Six-year*

experience: long-term disease control outcomes for partial breast irradiation using MammoSite balloon brachytherapy. 2010.
14. Maurer Foundation. https://www.maurerfoundation.org/a-brief-history-of-breast-cancer/
15. Matworks.*https://www.mathworks.com/help/matlab/call-mex-files-1.html?s_cid=wiki_mex_1*
16. Sang H. Shin, Wook J. Yoo, Kyoung W. Jang, Seunghyun Cho, Kum B. Kim, and Bongsoo Lee. *Development of an All-In-One Phantom and Scintillator radiation Sensor For Real-Time Monitoring of Source Position and Dose Distribution in High-Dose-Rate Brachytherapy*. February 26, 2016.
17. M. S. Naeini, Z. Han, D. Cutajar, S. Gautelli, M. Petasecca, M.L.F Lerch, D.R.Franklin, J. Jakubek, S. Pospisil, J. Bucci, M. Zaider, A.B. Rosenfeld. *BrachyView, A Novel Inbody Imaging System For HDR Prostate Bracytherapy: Design and Monte Carlo Feasibility Study*. June 17, 2013.
18. F. Foppiano, S. Agostinelli, S. Garelli, G. Paoli, P. Nieminen. *The Application of GEANT4 Simulation Code For Brachytherapy Treatment*. October 10, 2000.
19. Marc L. Dapas. *Review of The Emerging Medical Technologies Program*. Policy Issue March 9, 2018.
20. George M. Moore and Miles A. Pomper. *Permanent Risk Reduction: A Roadmap For Replacing High-Risk Radioactive Sources and Materials*. July 2015.
21. Canadian Nuclear Safety Commission. *National Sealed Source Registry (NSSR) and Sealed Source Tracking System (SSTS)*. Annual Report 2007.
22. Saree Alnaghy, Mitra S. Naeini, Daniel R.Franklin, Zhangbo Han, Dean L. Cutajar, Marco Petasecca, Michael Lerch, Anatoly B. Rosenfeld. *Analytical Modelling and Simulation of Single and Double Cone Pinholes For Real-Time In-Body Tracking of an HDR Brachytherapy Source*. June 2016.
23. Dr Annette Haworth. BrachyNext: In Vivo Dosimetry In Brachytherapy.
24. NationalCancerInstitute(NIH).https://www.cancer.gov/about-cancer/understanding/what-is-cancer.
25. Elodie Lugez. *Electromagnetic Tracking In Ultrasound-Guided High Dose Rate Prostate Brachytherapy*. March 2016
26. Nikolai Hungr, Michael Baumann, Jean A. Long, Jocelyne Troccaz. *A 3D Ultarsound Robotic Prostate Brachytherapy System With Prostate Motion Tracking*. June 2012
27. John A. Vargo, Vivek Verma, Hayeon Kim, Ronny Kalash, Dwight E. Heron, Ronald Johnson, and Sushil Beriwal. *Extended (5-year) Outcomes of Accelerated Partial Breast Irradition Using Mammosite Balloon Brachytherapy: Patterns of Failure, Patient Selection, and Dosimetric Correlates for Late Toxicity*. May 21, 2013.
28. The American Association of Physicists In Medicine. https://www.aapm.org/pubs/reports/detail.asp?docid=60 .
29. Varian Medical Systems Product Documentation. 2009.

VITA

Udeji Uchechukwu Leo was born in Lagos, Nigeria on May 1993. He completed High school Education in Penny International College, Lagos in August 2010. In January 2011, he started his undergraduate studies in Electronics engineering, at Infrastructure University Kuala Lumpur, Malaysia. He graduated with his BSc in Electronics Engineering in 2014.

In Fall 2015, he started his Masters program in Electrical and Computer Engineering in Virginia Commonwealth University, where he held several positions including that of an AV-technician at the student commons and a Teaching Assistant at the school of Engineering.

His team emerged first position of VCU's first Healthhacks competition in 2016, and he is currently a co-founder of AnyWearVR startup. An android app that help train children with autism before they go through actual treatment.